Doppler-Free Spectroscopy of Iodine at 739nm

by

Andrew Chew

A Senior Honors Thesis submitted to
the Department of Physics of
The College Of Literature, Science and the Arts
in The University of Michigan
in partial fulfillment
of the requirements for the degree of
Honors B.S. Physics
9th April 2008

To my Family

ACKNOWLEDGEMENTS

An undergraduate career can be regarded to be incredibly short especially one has finally reached at the end of the line. First off, I would like to thank Chris Monroe for allowing me to join his group in the fall of 2006. You have been a most helpful advisor and a great mentor who provided a lot of support and the opportunities for me to learn and understand new physics. You also provided the necessary paper work needed to allow me to continue working with the group when you moved the lab from Michigan to Maryland. I hope that I have contributed meaningfully to the group to your satisfaction.

Next, I would like to thank Ming-Shien Chang. Ming, you have been great mentor to me since I first joined the group and helped out in the Cadmium MOT experiment, guiding me through the first baby steps to becoming an experimentalist and helping me learn many new skills and new physics. Thanks for everything and best of luck with the Quantum Simulator Experiment. Hopefully things will turn out better with this experiment.

I also would like to thank Kathy-Ann Brickman who also worked on the MOT experiment and also guided me through some of the projects I worked on when I first joined the group. Thanks a lot. Many thanks also others with whom I have worked with and provided me help over the last 2 years: Mark Acton, Peter Maunz, Dave Moehring, Dan Stick, Jon Sterk, Steve Olmschenk, Simcha Korenblit, Dzmitry Matsukevich, Dave Hayes, Andrew Manning, Kihwan Kim, Dan Cook, Yisa Rumala

and Kelly Younge.

I also would like to thank a few other people, namely Mark Yeo, who was also a former member of the group, Teow Lim Goh and Chun Kiat Sim. They helped me get acquainted to the University of Michigan when I first arrived and we worked together doing Math or Physics. Best of luck to the future.

Last but not least, I would like to thank my family and friends, of whom though many are far away in Singapore, you provided me with moral and emotional support from so far away. Thank you.

TABLE OF CONTENTS

LIST OF FIGURES

Figure

LIST OF TABLES

Table

ABSTRACT

Doppler-Free Spectroscopy of Iodine at 739nm

by
Andrew Chew

In this thesis, we will present the results of the study of Iodine Doppler Free Saturated Spectroscopy performed at the 739.0289 nm region. We measured linewidth of the doppler free peaks and attempted to study the various inhomogeneous broadening effects typical in the gaseous phase, namely pressure broadening, power broadening and doppler broadening. We finally provide future steps for a robust iodine laser lock.

CHAPTER I

Introduction

1.1 Introduction

High resolution laser spectroscopies became powerful tools in atomic and molecular physics in recent years. Experiments of this class not only provide sensitive probes to study atomic and molecular structures in detail, but also that those techniques have revolutionized and set new standard of modern day metrology. Both goals are often very relevant and are usually approached iteratively. By that the acquired high resolution spectra provide absolute frequency references for the probe lasers, and the frequency stabilized lasers are then used to further manipulate the internal and external degrees of the atoms and molecules via spectroscopic means, such as laser cooling, optical pumping, or coherent manipulation. Laser stablization of 780 nm lasers used in Rubidium Bose Einstein Condensates can be achieved using Rubidium-87 as an atomic reference [24]. I_2 has been used as an atomic reference to stabilize He-Ne lasers at 633nm [4].

This thesis was derived from a subproject under a trapped ion quantum simulator project at the University of Maryland. In this thesis, the introduction will provide much of the motivation and basis behind the Iodine Doppler Free Spectroscopy. The first chapter will provide the theoretical background for doppler free spectroscopy,

and the second chapter will describe the experimental setup. The third chapter will show the experimental results and the last chapter will describe the next step for our spectroscopy.

1.2 Motivation

A classical computer is a computer, which has a memory consisting of bits which can hold 2 states, 0 and 1. A quantum computer on the other hand, has a memory in the form of qubits. Each can hold two states,$|0\rangle$ and $|1\rangle$, and a quantum superposition of both states. Richard Feynman presciently proposed in 1982 that a quantum computer would be ideal for simulating a quantum many-body system as the processing power required increases exponentially with the size of the system[8]. Such many-body systems are described as non-trackable, and simulations of such a systems with modern computers will quickly become prohibitively slow if not impossible. On the contrary, a quantum processor will be able to increase its processing power exponentially as the number of qubits, increases, thanks to the massive parallel computing built-in by the quantum phenomena, i.e., quantum superposition and quantum entanglement. Because of that, a quantum computer will be able to track down a many-body system that is considered non-trackable to a classical computer.

In recent years, trapped and laser cooled ions have been recognized as one of the most advanced scheme toward realizing a scalable quantum computer [3]. Almost without modifications, a trapped ion system can be used directly as a quantum simulator, in which one can simulate Heisenberg-like spin Hamiltonians[28]. While a two-ion quantum simulator has been realized, a quantum simulator utilizing few tens to few hundreds of ions will be one of the many first steps towards accomplishing this feat.

While a universal working Quantum Computer is many years away, one can build a quantum simulator that Feynman envisaged, which can be solved by using using a certain type of Hamiltonian[28]. In our research group, we focus our efforts on quantum computing and simulation, and quantum communication, by utilizing cold trapped singly-charged Ytterbium ions in a linear Paul trap. Ytterbium ion is considered laser friendly in that the the 6S $\leftrightarrow$ 6P cyclic transitions. Specifically, the $^2\mathrm{S}_{1/2} \leftrightarrow ^2\mathrm{P}_{1/2}$ transition of the $^{171}Yb^+$ is at 369.526 nm, and decent laser power can be obtained by doubling a laser at 739.052 nm. Our experiments employ diode systems, which are then doubled via ring cavity frequency doublers. Iodine molecule has been observed to have lines in the 739 nm region and would serve as a convenient frequency reference for stabilizing our diode lasers.

1.3 Trapping Ytterbium Ions for Quantum Computation

Ions stored in high frequency radio frequency (rf) traps have been demonstrated to have excellent properties, such as long coherence times and long trapping lifetimes, that make them attractive for scalable quantum computation [3, 18, 32]. Our group has demonstrated in S. Olmschenk et. al[27] that trapped ytterbium ($^{171}\mathrm{Yb}^+$) ions can be used as quantum bits for quantum information processing. We will also use the $^{171}\mathrm{Yb}^+$ ions for the Quantum Simulation experiment. $^{171}\mathrm{Yb}^+$ ion is loaded into a high frequency rf trap using photoionization. The oscillating rf-trap has the potential near the center given by [33]

$$\Phi = \frac{V_0 cos\Omega_T t + U_r}{2}\left(1 + \frac{x^2 - y^2}{R^2}\right) \tag{1.3.1}$$

Such an oscillating potential is essentially a saddle that forms a harmonic oscillator well. $^{171}\mathrm{Yb}^+$ ions are loaded into the trap through a resonant two-photon process by using two counterpropagating beams. One of which is a continuous wave(cw) diode

laser of wavelength 399 nm tuned near resonant to the $^1S_0 \rightarrow ^1P_1$ transition and the another is the 369.5 nm beam that is resonant to the $^2S_{1/2} \rightarrow ^2P_{1/2}$ transition, and has enough energy to drive the Ytterbium neutral to the continuum. An atomic beam of Yb neutrals is aimed at 90° at the 399 nm beam to reduce Doppler shifts and allow for isotopically selective loading. 935 nm and 638 nm beams are also aimed at the trapping region to prevent the ion from being trapped in the the metastable $^2D_{3/2}$ and $^2F_{7/2}$ states. Doppler cooling the ions requires a 369.5 nm beam to drive the $^2S_{1/2} \leftrightarrow ^2P_{1/2}$ transitions. It also aids detection as it generates fluorescence which can be collected and focused with an appropriate optics setup. 935 nm and 638 nm beams are used to pump back to the cyclic $^2S_{1/2} \leftrightarrow ^2P_{1/2}$ transitions any of the ions that decayed into the metastable $^2D_{3/2}$ and $^2F_{7/2}$ states. Subsequently, the Ytterbium Qubit will be prepared and manipulated by the 369.5 nm, 935 nm and 638 nm laser beams. More details on the cooling arrangement and Qubit manipulation can be found in S. Olmschenk et. al [27].

The 369.5 nm beam is produced by frequency doubling a 739 nm laser beam produced by an amplified cw diode laser from Toptica. An advantage of using a 739 nm laser is that it can be stabilized by a molecular iodine reference[27]. This thesis is thus concerned with the doppler free spectroscopy of iodine at 739 nm for use in stabilization of our 739 nm cw diode laser.

1.4 The Iodine Molecule

The Iodine I molecule is a well studied diatomic molecule with numerous old literature [13, 11, 9, 10, 12, 2], detailing the absorption lines from 7220 cm^{-1} to 23800 cm^{-1}. which are equivalent to 420.168nm to 1385.042nm. The emissions in the visible spectrum to near infrared(IR) are due to transitions from the $B^3\Pi_{0-u} \rightarrow$

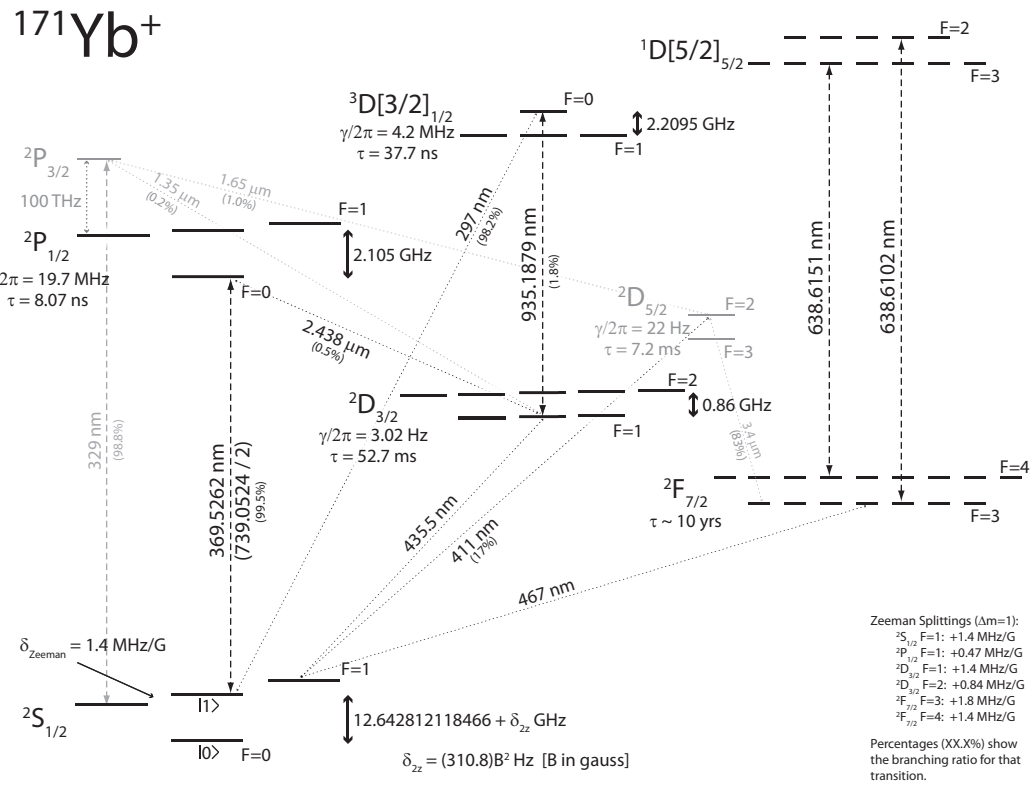

Figure 1.1: Ytterbium fine and hyperfine structure. The complete level scheme, including the hyperfine structure, of Ytterbium which is exploited for ion trapping. A 369.5 nm laser is essential for driving the $^2S_{1/2} \rightarrow ^2P_{1/2}$ transitions for ionizing the Ytterbium neutral to the continuum and also to cool the atom. The 369.5nm laser is also used for state detections and for preparing and manipulating the Ytterbium Qubit.

X $^1\Sigma_g^+$ manifold ([17]). Molecular iodine is often selected as a frequency reference for wavelengths from the near-infrared (e.g., 830 nm [21]) to the visible spectrum (e.g., 633 nm [16]) to the disassociation limit at 499.5 nm because of the density of narrow absorption lines in this region[14, 11]. These lines can serve as excellent frequency references for laser stabilization to a few parts in 10^{-9} or better[7]. However, data on the transitions involved in producing the spectrum for the regions 667 nm to 776 nm and the 514 nm to 526 nm is generally scarce [19] beyond what data was provided by the iodine atlas by Gerstenkorn and Luc (GL atlas [11, 10]) likely due to the weak lines at room temperature. It is not altogether certain whether the lines around the 739nm region (13530.0936cm^{-1}, 13530.1934cm^{-1} and 13530.6745cm^{-1} [14]) are

a result of a two level system or three level or some more complicated system.

Regardless, we should expect that that the infrared lines of the Iodine spectrum are a result of vibrational and rotational energy level transitions in addition to the electronic energy level transitions[17]. Transitions between the vibrational energy levels give rise to fine structure while rotational energy levels give rise to the hyperfine structure. The energy involved in a transition is given as a sum of that of all three types of transitions[17]. Hence, in terms of the transition frequencies, the energy is given as:

$$E_{transition} = \hbar\omega = \hbar(\omega_r + \omega_v + \omega_t) \tag{1.4.1}$$

where ω_t, ω_v and ω_r are the frequency contributions due to the electronic energy level transitions, vibrational energy level transitions and rotational energy level transitions respectively. The vibrational energies could be modeled by the simple harmonic oscillator model. As numerous textbooks on Quantum Mechanics, such as the one by Griffiths[15] and Sakurai[29], would have it, solving the Schrödinger equation with potential $V(r) = \frac{1}{2}kx^2$ where k is the force constant would yield the vibrational energy levels E_v to be

$$E_v = (n + \frac{1}{2})\hbar\omega_k \tag{1.4.2}$$

where ω_k is the frequency of the vibration. These are very simplistic models and in the case of iodine, they might be too simple to model. In the case of vibrational energies, it might be more appropriate to use a Anharmonic Oscillator well instead[17]. For rotational energies, we might need to use the nonrigid rotator or symmetric top[17]. Nevertheless, they give us some idea of what we should expect in our spectrum.

The simplest model of a rotating molecule is to regard the molecule as a rigid

rotator[17]. The energy of rotation E_r of a rigid body is given by

$$E_r = \frac{1}{2} I \omega_r^2 = \frac{L^2}{2I} \tag{1.4.3}$$

where I is the moment of inertia of the system about the axis of rotation and ω_r is the angular velocity and L is the angular momentum of the system, given by $L = I\omega_r$. The moment of inertia is given to be

$$I = \mu r^2 \tag{1.4.4}$$

where μ is the reduced mass of the system. Solving the Schrödinger equation in spherical coordinates yields $L = J(J+1)\hbar^2$ where J is the rotational energy quantum number. So effectively the rotational energies are given by

$$E_r = \frac{J(J+1)\hbar^2}{2I} \tag{1.4.5}$$

Thhe transitions we are trying to examine are not at the ground vibrational levels, and thus the population of molecules at the required vibrational levels are not sufficiently populated to produce the spectrum at around 739nm. The iodine thus requires substantial heating to about $500°C$[19] to sufficiently populate those states which produce the spectrum around 739nm. The number of molecules dN that has energy between E and E + dE at thermal equilibrium is given by the Boltzmann distribution [17]

$$\mathrm{d}N \propto e^{-E/kT} \mathrm{d}E \tag{1.4.6}$$

In the case of vibrational energy levels, the number of molecules N_v in state n is [17]

$$N_v = \frac{N}{Q_v} e^{-E_n/kT} \tag{1.4.7}$$

where k is the Boltzman constant and N is the total number of molecules while Q_v is the partition function given by $Q_v = 1 + e^{-E_1/kT} + e^{-E_2/kT} + ...$

In the case of rotational energy levels, it is given by [17]

$$\mathrm{d}N_i = N\frac{g_i}{Z}e^{-E_i/kT} \tag{1.4.8}$$

where $g_i = 2J_i + 1$ is the statistical weight that gives the number of degenerate sublevels at the level $|i\rangle$ with total angular momentum J_i and the partition function $Z = \sum_i g_i e^{-E_i/kT}$ is the normalizing constant.

Hence, the higher temperature, the more populated the higher energy states are. In the case of a two level system, we would want the ratio between the population at the excited state N_2 and the population between the ground state N_1 to be

$$N_2/N_1 \propto e^{-(E_2-E_1)/kT} = e^{-1} \tag{1.4.9}$$

Otherwise, there will not be sufficient transitions and thus the doppler signal would be too weak for us to pick out.

CHAPTER II

Theory of Frequency Modulated Doppler Free Spectroscopy

Of the many ways to implement Doppler free Spectroscopy, one of them is to have two counter propagating beams, a stronger pump and a weaker probe beam, going through a vapor cell heated to a certain temperature. A single laser beam alone, tuned to the right resonant frequency of the atoms, would on its own, produce a doppler broadened absorption spectrum. Having two laser beams, each tuned to the same resonant frequency, would instead introduce doppler free dips in the doppler broadened absorption spectrum corresponding to the frequency of the transitions. The advantage of Doppler Free Spectroscopy is such that, combined with frequency modulation of the pump beam, the resolution of the weaker lines in the spectrum of a given atom would be enhanced. This signal is a result of many underlying processes, namely doppler broadening, pressure broadening, and power broadening, that will now be examined in detail in this chapter.

2.1 The Doppler Free Signal

2.1.1 Lambert-Beer's Law

The Lambert-Beer's law holds when the absorption is linear. The vapor cell could be regarded as a dielectric medium and the intensity of the laser decreases along the

length of the cell by [23]

$$dI = -\alpha(\omega) I dz \tag{2.1.1}$$

where $\alpha(\omega) = \sigma(\omega)n$ and $\sigma(\omega)$ is the cross section of the interaction between the photon and the atom as a function of frequency ω and n is the population density. Solving the differential equation, and assuming that the absorption coefficient α is independent of intensity, we have

$$I(z) = I_0 e^{-\alpha(\omega)nz} \tag{2.1.2}$$

Of particular note would be the fact that the doppler free signal would grow stronger as the length of the interaction increases. However, α not only has frequency dependencies, but also laser intensity dependencies which invalidate Eqn. 2.1.2.

2.1.2 Natural Linewidth

The power spectrum of the emitted of light from a stationary excited atom could be modeled by considering the excited atomic electron as a Lorentz oscillator, namely a classical damped simple harmonic oscillator. Define $\omega_0 = \sqrt{k/m}$ as the natural frequency of the oscillation of the oscillator, where k is the the force constant and m the mass of the oscillator. The differential equation of motion is given by[5]

$$\ddot{x} + \gamma_0 \dot{x} + \omega_0^2 x = 0 \tag{2.1.3}$$

where γ_0 as the damping constant. Note that ω_0 corresponds to the central frequency of the transition $\omega_{if} = (E_f - E_i)/\hbar$. Taking $\omega_0 \gg \gamma_0$, we can solve the above differential equation, by applying the trial solution $x = x_0 e^{i\omega t}$ and taking the real component of the solution. Substituting and solving with the given initial conditions yields

$$x(t) = x_0 e^{\frac{\gamma_0 t}{2}} \left(\cos \omega' t + \frac{\gamma_0}{2\omega'} \sin \omega' t \right) \tag{2.1.4}$$

where $\omega' = \sqrt{\omega_0^2 - \gamma_0^2/4}$ If the damping is small, we can neglect the sine term and $\omega' \sim \omega_0$. The solution then reduces to

$$x(t) = x_0 e^{\frac{\gamma_0 t}{2}} (\cos \omega_0 t) \tag{2.1.5}$$

Performing a Fourier Transformation and using Euler's formula to obtain the spectral distribution of the photons emitted yields,

$$A(\omega) = \frac{x_0}{2\sqrt{2\pi}} \left(\frac{1}{i(\omega - \omega_0) + \gamma_0/2} + \frac{1}{i(\omega + \omega_0) + \gamma_0/2} \right) \tag{2.1.6}$$

Since Intensity $I \propto x^2$, one would expect that in the frequency space, $I \propto |A(\omega)|^2$. Hence, if we focus on the region $\omega_0 \approx \omega$, we can neglect the $(\omega_0 + \omega)$ terms. Thus,

$$I(\omega - \omega_0) == C' \left(\frac{\gamma_0/2\pi}{(\omega - \omega_0)^2 + (\gamma_0/2)^2} \right) \tag{2.1.7}$$

Where C' is a proportional constant. The intensity I is a normalized Lorentzian curve and the Full Width Half Maximum(FWHM), which gives the frequency range at which the intensity is half its maximum (which is $\frac{2}{\gamma_0 \pi}$), is γ_0. An example of a Lorentzian curve is depicted in Fig. 2.1. An electron excited by an incident photon

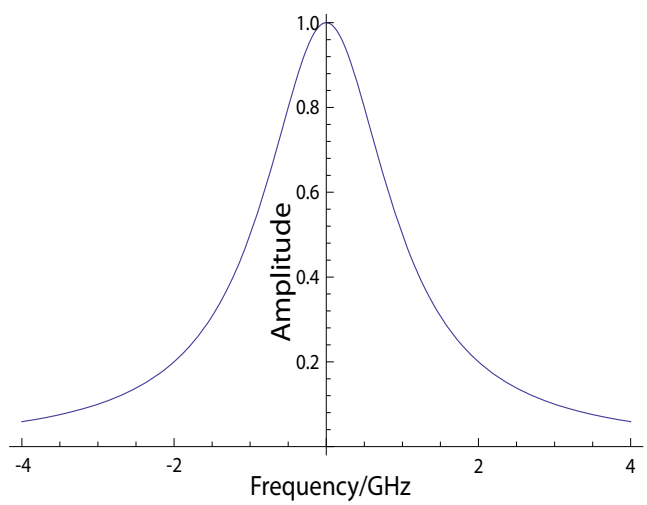

Figure 2.1: A Lorentzian Emission Profile

tuned close to the same energy transition could also be modeled with a similar

differential equation [5]. An electron of charge e is excited by a weak electric field $E = E_0 e^{i\omega t}$ with the following equation of motion for the weakly driven oscillator[5]

$$\ddot{x} + \gamma_0 \dot{x} + \omega_0^2 x = \frac{qE_0}{m} e^{i\omega t} \tag{2.1.8}$$

The above equation can be solved by introducing a particular solution $x = e^{i(\omega+\tau)t}$, and the solution is given as

$$x(t) = \frac{qE_0 e^{i\omega t}}{m\left(\omega_0^2 - \omega^2 + i\gamma_0\omega\right)} \tag{2.1.9}$$

To find the intensity as a function of frequency, we need to use the Fourier transform to solve the above differential equation and obtain the solution in the frequency domain. Taking $|\omega - \omega_0| \ll \omega_0$, we have [5]

$$I(\omega) \propto \frac{\gamma_0/2}{((\omega_0 - \omega)^2 + (\gamma_0/2)^2)} \tag{2.1.10}$$

We note immediately that $I(\omega)$ is a Lorentzian and is similar to Eqn.2.1.7 with the same FWHM of γ_0. We thus should expect that any stationary excited atom to emit light that has a Lorentzian line profile with a linewidth identical to that of the natural linewidth. Such a profile is depicted in Fig. 2.2. However, in reality, there are a combination of effects that might broaden the linewidth and modify the shape of the signal. This will be discussed in the in the subsequent sections.

2.2 Inhomogenous Broadening

Inhomegenous broadening effects arise from the fact that atoms are not stationary and are constantly moving and collide with each other, leading to collision and doppler broadening. Further, broadening effects will also arise when the gas cell is sufficiently saturated when the energy levels involved become evenly populated. Such effects may or may not appear in the signal we observe, though doppler broadening will definitely observed given that it is an intrinsic part of our experiment.

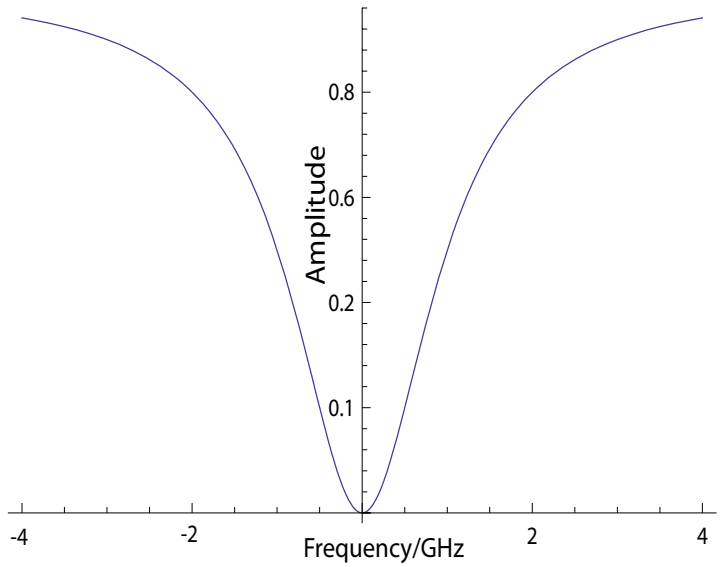

Figure 2.2: A Lorentzian Absorption Profile

2.2.1 Doppler Broadening

The frequency of incident photons ω is doppler shifted in the rest frame of the molecule traveling in the velocity vector $\mathbf{v}$ to ω'. Define $\mathbf{k}$ here to be the wave vector of the incident photon.

$$\omega' = \omega - \mathbf{k} \cdot \mathbf{v} \tag{2.2.1}$$

In the lab frame, a photon of frequency ω'' with k wave vector emitted from a molecule is doppler shifted by

$$\omega = \omega'' + \mathbf{k} \cdot \mathbf{v} \tag{2.2.2}$$

To simplify matters, consider only molecules traveling in the z-direction with velocity v_z. If the frequency of the photon ω' is tuned to ω_0 which is one of the resonant frequency of the molecules, the absorption frequency ω_a in the lab frame is given by

$$\omega_a = \omega_0 \left(1 + \frac{v_z}{c}\right) \tag{2.2.3}$$

Thus we will inevitably see a doppler broadening of the Lorentzian lineshape. In thermal equilibrium at a given different temperature T, the molecules follow a Maxwell-

Boltzmann velocity distribution and thus the number of molecules $n_i(v_z)dv_z$ at a certain energy level E_i with velocity along the z-direction between v_z and $v_z + dv_z$ is given by [5][31]

$$n_i(v_z)\mathrm{d}v_z = N_i\sqrt{\frac{m}{2kT\pi}}\exp\left(-\frac{mv_z^2}{2kT}\right)\mathrm{d}v_z \tag{2.2.4}$$

where $N_i = \int_{v_z} n_i(v_z)\mathrm{d}v_z$ and m is the mass of the molecule. Rearranging Eqn. 2.2.3, we have

$$v_z = c\left(\frac{\omega_a - \omega_0}{\omega_0}\right) \tag{2.2.5a}$$

$$\mathrm{d}v_z = \frac{c}{\omega_0}\mathrm{d}\omega_a \tag{2.2.5b}$$

Substituting Eqn. 2.2.5b into Eqn. 2.2.4, we obtain the number distribution of the molecules with absorption frequencies differing from ω_0 in the interval ω and $\omega + \mathrm{d}\omega$.

$$n_i(\omega_a)\mathrm{d}\omega_a = N_i\frac{c}{\omega_0}\sqrt{\frac{m}{2kT\pi}}\exp\left(-\left(\frac{c(\omega_a - \omega_0)}{\omega_0}\right)^2\frac{m}{2kT}\right)\mathrm{d}\omega_a \tag{2.2.6}$$

The intensity of the signal would naturally be proportional to the population of molecules that interact with the laser. The expected doppler broadened profile should be thus of form

$$I_D(\omega_a) = I_0\exp\left(-\left(\frac{c(\omega_a - \omega_0)}{\omega_0}\right)^2\frac{m}{2kT}\right) \tag{2.2.7}$$

which is a Gaussian. The doppler width γ_D is then

$$\gamma_D = \sqrt{\frac{(8\ln 2)kT}{mc^2}}\omega_0 \tag{2.2.8}$$

Normalizing the Gaussian leads to [31]

$$I_D(\omega_a) = \left(\frac{4\ln 2}{\pi\gamma_D}\right)^{1/2}\exp\left(-(4\ln 2)\left(\frac{c(\omega_a - \omega_0)}{\gamma_D}\right)^2\right) \tag{2.2.9}$$

To find the resulting signal, take a convolution of Eqn. 2.2.9 and Eqn. 2.1.7 and obtain

$$\begin{aligned} I_v(\omega) &= \int I(\omega - \omega_a)I_D(\omega_a)\mathrm{d}\omega_a \\ &= C\int_{\infty}^{\infty}\frac{\gamma_0/2}{((\omega_0 - \omega_a)^2 + (\gamma_0/2)^2)}\exp\left(-(4\ln 2)\left(\frac{c(\omega_a - \omega_0)}{\gamma_D}\right)^2\right)\mathrm{d}\omega_a \end{aligned} \tag{2.2.10}$$

Where C is some normalizing constant. Eqn.2.2.10is essentially a Voigt Lineshape which is quite complicated to solve analytically although numerical approximations are possible. However, given that the doppler effects will be quite large even at room temperature, we might however be able to find approximations for it. If $\gamma_0 \ll \gamma_D$, we might approximate the Lorentzian as a delta function [31] and produce:

$$\begin{aligned} I_v(\omega) &= C \int_{\infty}^{\infty} \delta(\omega - \omega_a) \exp\left(-(4\ln 2)\left(\frac{c(\omega_a - \omega_0)}{\gamma_D}\right)^2\right) \mathrm{d}\omega_a \\ &= C' \exp\left(-(4\ln 2)\left(\frac{c(\omega - \omega_0)}{\gamma_d}\right)^2\right) \end{aligned} \tag{2.2.11}$$

It is then valid to approximate the possible doppler profile with a Gaussian with linewidth γ_D.

2.2.2 Pressure Broadening

Pressure broadening, or collision broadening in some literature, arises from collisions between molecules in the vapor cell. Collisions whether elastic or inelastic, will both broaden the linewidth.

Returning to the damped oscillator model in section 2.1.2, elastic collisions do not induce energy transfer, and therefore will not alter the amplitude of the oscillations. However, the phase can be shifted due to the frequency shift during the collisions. Elastic collisions cause a shift in not only in the linewidth, but also a shift in the resonance peak. Ignoring any doppler effects, we have a lorentzian of the form [5]:

$$I_c(\omega) = \frac{I_0}{2\pi} \frac{(\gamma_0/2 + N\bar{v}\sigma_b)^2}{(\omega - \omega_0 - N\bar{v}\sigma_s)^2 + (\gamma_0/2 - N\bar{v}\sigma_b)^2} \tag{2.2.12}$$

where σ_b and σ_s are cross sectional constants to be determined through experimentation, and N is the particles per unit volume and $\bar{v}$ is the mean relative velocity.

Inelastic collisions on the other hand, reduce the number of atoms in the excited state. The effect on this results in the damping constant is increased by γ_{col}^{inel}. Hence,

we finally have [5]

$$I_c(\omega) = \frac{I_0}{2\pi} \frac{\gamma_0 + \gamma_{col}^{inel} + N\bar{v}\sigma_b}{(\omega - \omega_0 - N\bar{v}\sigma_s)^2 + \left(\gamma_0/2 + \gamma_{col}^{inel} + N\bar{v}\sigma_b\right)^2} \tag{2.2.13}$$

Thus the total linewidth γ_c is

$$\gamma_c = \gamma_0/2 + \gamma_{col}^{inel} + 2N\bar{v}\sigma_b \tag{2.2.14}$$

2.2.3 Power Broadening

Assume that the energy level transitions $|g\rangle \rightarrow |e\rangle$ in question form a two level system. We then have the Optical Bloch equations with spontaneous emission [23]

$$\frac{\mathrm{d}\rho_{ee}}{\mathrm{d}t} = \gamma\rho_{ee} - \frac{i}{2}\left(\Omega^*\rho_{eg} - \Omega\rho_{ge}\right)) \tag{2.2.15a}$$

$$\frac{\mathrm{d}\rho_{gg}}{\mathrm{d}t} = \gamma\rho_{ee} - \frac{i}{2}\left(\Omega\rho_{ge} - \Omega^*\rho_{eg}\right)) \tag{2.2.15b}$$

$$\frac{\mathrm{d}\rho_{eg}}{\mathrm{d}t} = -\left(\frac{\gamma}{2} - i(\omega - \omega_0)\right)\rho_{eg} + \frac{i\Omega}{2}\left(\rho_{ee} - \rho_{gg}\right) \tag{2.2.15c}$$

$$\frac{\mathrm{d}\rho_{ge}}{\mathrm{d}t} = -\left(\frac{\gamma}{2} + i(\omega - \omega_0)\right)\rho_{ge} + \frac{i\Omega^*}{2}\left(\rho_{ee} - \rho_{gg}\right) \tag{2.2.15d}$$

where $\Omega = -eE_0/\hbar\langle e|r\rangle$ is the Rabi frequency and γ here is linewidth of the decay from the excited state. ρ_{ee} and ρ_{gg} are the probability of an atom being in the excited and ground state respectively, and are proportional to the population in both the excited and ground states. ρ_{ge} and ρ_{eg} can be considered as a form of coupling between the ground and excited state. Let $\rho_D = \rho_{ee} - \rho_{gg}$ be the population difference between the excited state and the ground state. ρ_D is then

$$\frac{\mathrm{d}\rho_D}{\mathrm{d}t} = -\gamma_0\rho_D - i\left(\Omega\rho_{eg}^* - \Omega^*\rho_{eg}\right) + \gamma_0 \tag{2.2.16}$$

The above equations can be solved by taking the steady state case with both derivatives equal zero. We then have [23]

$$\rho_D = \frac{1}{1+s} \tag{2.2.17a}$$

$$\rho_{eg} = \frac{i\Omega}{2(\gamma_0/2 - i(\omega - \omega_0))(1+s)} \tag{2.2.17b}$$

$$\text{where } s = \frac{|\Omega|^2/2}{\gamma_0^2/4 + (\omega - \omega_0)^2} = \frac{I/I_s}{\gamma_0^2/4 + (\omega - \omega_0)^2} \tag{2.2.17c}$$

$$\text{where } I_s = \frac{\pi hc}{3\lambda^3\tau} \tag{2.2.17d}$$

where τ is the lifetime and λ is the wavelength of the transition and I is the intensity of the beam. I_s is the saturation intensity and s is the saturation parameter. Let $s_0 = I/I_s$. With these equations in hand, we can now examine how the population in the excited state varies. We expect that when the transitions are driven by a laser beam of high intensity, both excited and ground states are equally populated, i.e. $\rho_D = 0$. Thus, we would have the population ρ_{ee} to be [23]

$$\rho_{ee} = \frac{1}{2}(1 - \rho_D) = \frac{s_0}{1 + s_0 + (2(\omega - \omega_0)/\gamma_0)^2} \tag{2.2.18}$$

where when $\rho_D \to 0$, $\rho_{ee} = 1/2$. Since the population decays at a rate γ_0, the scattering rate $\gamma_S = \gamma_0\rho_e$. As s_0 gets large, we can write [23]

$$\gamma_S = \left(\frac{s_0}{1+s_0}\right)\left(\frac{\gamma_0/2}{1 + (\omega - \omega_0)^2/((\gamma_0/2)^2(1+s_0))}\right) \tag{2.2.19}$$

Thus, comparing γ_S to Eqn. 2.1.7, we recognize that the effective linewidth γ_p of the Lorentzian is

$$\gamma_p = \gamma_0\sqrt{1+s_0} \tag{2.2.20}$$

Thus, with greater laser intensity, we will see further widening of the linewidth. However, it should be noted that the gas cell must be sufficiently saturated. Otherwise, this broadening will not be observed.

One way to quantify power broadening instead is to attempt to measure signal intensity and find the saturation intensity I_s. Consider again the scattering rate γ_S as a function of only intensity I and set $\omega = \omega_0$. Thus we have

$$\gamma_S = \gamma_0/2\left(1 - \frac{I_s}{I_s + I}\right) \tag{2.2.21}$$

To find the saturation intensity, set $\gamma_S = \gamma_0/4$ which is half the maximum scattering rate. Thus, with some rearranging, the corresponding intensity is thus I_s.

2.3 Hole Burning and Velocity Selection

The resolution of the spectroscopy is affected by the broadening effects mentioned in this chapter. Doppler Broadening, in particular, is one of the most dominant broadening effects that decreases resolution of the spectroscopy. To counter this, we perform velocity selection, whereby only molecules in a certain velocity class can be excited by the counter-propagating laser beams. One beam is the pump beam and the other is the probe beam, and the pump beam is typically 5-10 times more intense than the probe beam. Thus only molecules with near zero velocity can interact with both pump and probe beams.

To understand how velocity selection works in the context of Doppler Free Spectroscopy, let us consider a number of scenarios. Note that velocity components of molecules in the x and y direction have no bearing on the linewidth broadening. Given the absorption profile in the rest frame of the molecules has a natural linewidth γ_0, we should expect the frequency range of the laser that can interact with the molecules to be approximately $\omega_0 \pm \gamma_0/2$.

Consider a pump beam and probe beam both tuned to the exact same frequency while sweeping over a range of frequencies which include the the transition frequency $\omega_0 = (E_f - E_i)/\hbar$ in a two level system. Assume also, that the laser has a small linewidth such that we can consider it a delta function and that laser intensity is constant (in reality, it is a Gaussian beam). In the lab frame, the absorption frequency ω_a of the molecule has been shifted according to Eqn. 2.2.3 and the incident photons in the rest frame of the molecules would be shifted accordingly.

The range of velocities that allow the incident photons in the pump beam when it to interact with the molecules when it is at a frequency ω are

$$\left(-1+\frac{\omega_0-\gamma_0/2}{\omega}\right) \leq \frac{v_{z,pump}}{c} \leq \left(-1+\frac{\omega_0+\gamma_0/2}{\omega}\right) \tag{2.3.1}$$

Correspondingly, for the probe beam, the range of velocities are

$$\left(1-\frac{\omega_0-\gamma_0/2}{\omega}\right) \leq \frac{v_{z,probe}}{c} \leq \left(1-\frac{\omega_0+\gamma_0/2}{\omega}\right) \tag{2.3.2}$$

The overlap between the two ranges give the very small range of velocities that will cause the molecules to interact with both probe and pump beams, with a center velocity of 0. For example, if we tune the laser frequency to exactly ω_0, the common frequency would be $\gamma_0/2\omega \leq \frac{v_z}{c} \leq \gamma_0/2\omega$. The center frequency of the interaction remains the same at ω_0. Molecules with velocity that fall outside the overlap between the above two ranges will not interact with the probe beam.

Since the pump beam is expected to be above saturation intensity. Thus, the pump beam excites a greater proportion of population to the relative excited state of the two level system. Thus, the population of molecules with velocity falling in both the two ranges of velocities above available to interact with the much weaker probe will inevitably be reduced. Hole burning of the Voigt line profile (see Eqn. 2.2.11 will occur in the regions where the frequency of the laser matches the absorption frequencies of the molecule in the lab frame. Note that the probe beam must be be weaker so that it will not cause further saturation and power broadening of the linewidths.

In our experimental setup, the pump laser was sent through an Acousto-Optic Modulator (AOM) before going through the vapor cell. The pump laser frequency is thus expected to experience a shift of $-\omega_f$ and thus the pump laser frequency is

$$\omega = \omega_{probe} - \omega_f \tag{2.3.3}$$

To find the velocity class that interact with both beams in this case, simply substitute the above relation into Eqn.2.3.1 and Eqn. 2.3.2 and then check for the overlapping range. This range also gives the range of absorption frequencies by substituting the upper and lower bounds of the velocity range into Eqn. 2.2.3. We thus have

$$-1 + \frac{\omega_0 + \gamma_0/2}{\omega_{probe} - \omega_f} \leq \frac{v_{z,pump}}{c} \leq -1 + \frac{-\Delta + \gamma_0/2}{\omega_{probe} - \omega_f} \tag{2.3.4a}$$

$$1 - \frac{\omega_0 + \gamma_0/2}{\omega_{probe}} \leq \frac{v_{z,probe}}{c} \leq 1 - \frac{\omega_0 - \gamma_0/2}{\omega_{probe}} \tag{2.3.4b}$$

Again, the overlap of the two velocity ranges above will dictate the range of velocities that will interact with both the pump and probe beams. To find the central velocity at which the molecule would be resonant to both the pump and probe beams, we need to consider how the frequency of each beam is shifted due to the doppler effect. Let ω'_{probe} and ω'_{pump} be the frequency of the probe laser and pump laser in the rest frame of the molecule. Thus

$$\omega'_{probe} = \omega_{probe}\left(1 - \frac{v_z}{c}\right) \tag{2.3.5a}$$

$$\omega'_{pump} = (\omega_{probe} - \omega_f)\left(1 + \frac{v_z}{c}\right) \tag{2.3.5b}$$

Setting $\omega'_{probe} = \omega'_{pump} = \omega_0$, we obtain

$$v_z = \frac{c\omega_f}{2\omega_{probe} - \omega_f} \tag{2.3.6}$$

The corresponding value of ω_{probe} in terms of the resonant frequency can then be obtained by substituting Eqn. 2.3.6 into Eqn. 2.3.5b with $\omega'_{pump} = \omega_0$, and then we obtain

$$\omega_{probe} = \frac{2(\omega_0 + \omega_f) + \sqrt{4(\omega_0 + \omega_f)^2 - 8\omega_0\omega_f}}{4} \tag{2.3.7}$$

In our experiment, ω_f is 80 MHz and since we would expect that ω_{probe} should be close to the resonant frequency ω_0 at 406 THz, v_z $10ms^{-1}$. Hence, we do not expect

the velocity of the molecules to change the resonant frequency in the lab frame due to the doppler effect as the average velocity is effectively zero. Essentially, when the probe and pump beam interact with the molecule when

$$\omega_{probe} \approxeq \omega_0 + \frac{\omega_f}{2} \tag{2.3.8}$$

Further, taking a derivative of v_z with respect to ω_{probe}, we have

$$\delta v_z = -\frac{c\omega_f}{(2\omega_{probe} - \omega_f)^2}\delta\omega_{probe} \tag{2.3.9}$$

Adding a small perturbation $\delta\omega_{probe}$ to ω_{probe} in Eqn:2.3.5a then yields,

$$\omega'_{probe} = (\omega_{probe} + \delta\omega_{probe})\left(1 - \frac{v_z + \delta v_z}{c}\right) \tag{2.3.10}$$

Substituting Eqn. 2.3.9 to Eqn. 2.3.10, and after some manipulation, we yield

$$\begin{aligned}\omega'_{probe} = \omega_0 + \delta\omega_{probe} + \left(-\frac{\omega_f}{2\omega_{probe} - \omega_f}\delta\omega + +\frac{\omega_f\omega_{probe}}{(2\omega_{probe} - \omega_f)^2}\right)\delta\omega_{probe} \\ + \frac{\omega_f}{(2\omega_{probe} - \omega_f)^2}\delta\omega_{probe}^2\end{aligned} \tag{2.3.11}$$

If $\delta\omega_{probe}$ $\pm\gamma/2$ and $\gamma \ll \omega_{probe}$ ($\gamma \sim MHz$), the above equation reduces to

$$\omega'_{probe} \approxeq \omega_0 \pm \frac{\gamma}{2} \tag{2.3.12}$$

Solving for ω'_{pump} yields a similar result. This tells us that the central frequency and the linewidth of the absorption profile of the velocity class will correspond to the resonant frequency and the linewidth of the molecules. The velocity of the molecules is small enough that it is possible to neglect the possible doppler broadening of the natural linewidth. As such, we may write the signal in the form:

$$I_{D.F}(\omega) = A\left(\frac{s_0}{1+s_0}\right)\left(\frac{\gamma_0/2}{1 + (\omega - \omega_0)^2/((\gamma_0/2)^2(1+s_0))}\right) \tag{2.3.13}$$

where A is a constant proportional ρ_D (the population difference). To obtain the final signal, we need to account for both the doppler signal and the doppler free signal[5].

We then expect the final result, excluding any power and pressure broadening, to be

$$I_{Lock}(\omega) = \left(1 - I_0 \exp\left(-(4\ln 2)\left(\frac{c(\omega-\omega_0)}{\gamma_d}\right)^2\right)\right) \times \left(A\frac{s_0}{1+s_0}\right)\left(\frac{\gamma_0/2}{1+(\omega-\omega_0)^2/((\gamma_0/2)^2(1+s_0))}\right) \tag{2.3.14}$$

Note that the could be possible power and pressure broadening of the natural linewidth, and as such, γ_0 should be replaced with the appropriate linewidth as necessary. The doppler free peak is depicted in Fig. 2.3. In addition to the doppler free peaks,

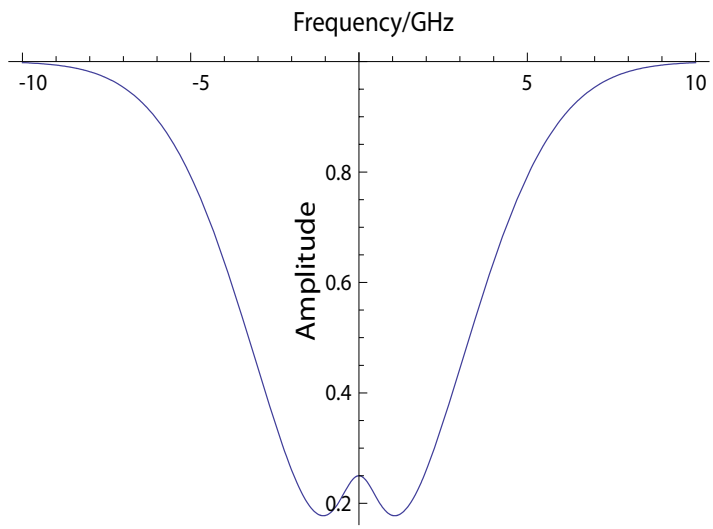

Figure 2.3: A Doppler Free Peak in Doppler Profile. Notice that the peak is small compared to the rest of the Gaussian absorption profile

we need to also examine the occurrence of crossover signals [5]. Crossover signals occur in multi-level systems where there is a common ground or upper state and the frequency of these signals is the average of the two levels which contribute to the crossover signal. Consider then a three-level system as shown in Fig. 2.8.

The frequency of the transition to the upper state 1 to be ω_1 and upper state 2 to be $\omega_1 + \Delta$, where $\Delta \ll \omega_1$. Because Δ is small, an incident photon could be doppler shifted in the rest frame of atoms traveling at a certain velocity such that the photon could excite the atoms to the 2 upper states simultaneously. Thus, a crossover peak is produced in the doppler absorption profile. To determine the exact

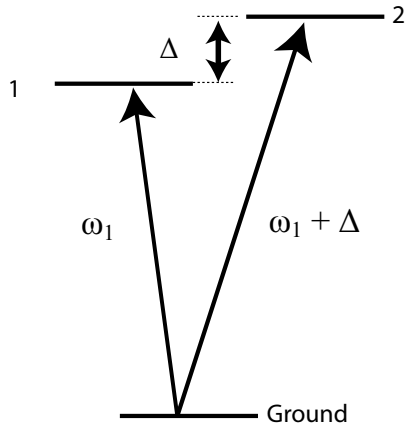

Figure 2.4: A possible 3 energy level system.The frequencies of the two transitions are ω_1 and $\omega_1 + \Delta$ where Δ is the difference in frequency between the two transitions. We would thus expect a cross over peak between the two upper energy levels, i.e.$\omega_1 + \Delta/2$. This is in addition to the two doppler free peaks we should see as a result of the transitions to the 2 upper level states.

central frequency of the crossover signal, let us return to Eqn. 2.3.5b and 2.3.5a. Let $\omega'_{pump} = \omega_1 + \Delta$ and $\omega'_{probe} = \omega_1$. Solving both Eqn. 2.3.5b and 2.3.5a for ω_p yields

$$\omega_p = \frac{(2\omega_0 + \omega_f + \Delta) + \sqrt{4(2\omega_0 + \omega_f + \Delta)^2 - 8\omega_0\omega_f}}{4} \tag{2.3.15}$$

Since $\omega_f \ll \Delta$, we can approximate ω_p to

$$\omega_p \simeq \omega_0 + \frac{T}{2} \tag{2.3.16}$$

which is where we expect the crossover peak to show. If we have more than 2 upper level or ground states. In between any two of the energy levels would have a crossover peak.

2.4 Frequency Modulation and Detecting the Signal

For effective detection of weak signals, the process of modulation-demodulation must be used. The pump beam will be frequency modulated using an AOM as mentioned before, and a Lock-in Amplifier will be used to demodulate the signal received from the photodiode. The Lock-in Amplifier works on the principle of

frequency modulation-demodulation[5] and is a phase sensitive detector. It consists of a demodulator in the form of a mixer, where the error signal $\alpha(\omega)$ is multiplied by the reference signal. The mixed signal is subsequently passed through a low pass filter to filter out the high frequency noise. The process is shown graphically in Fig.2.5.

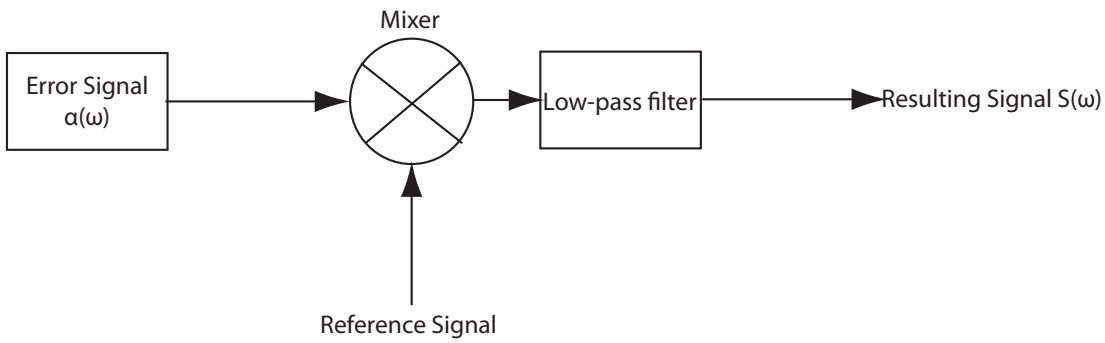

Figure 2.5: Block Diagram describing the processes in the Lock-in Amplifier. A Lock-in Amplifier consists consists of a demodulator in the form of a mixer and low pass filter. The input signal $\alpha(\omega)$ is multiplied with the reference signal, and is subsequently passed through a low pass filter to filter out the high frequency noise to produce S(ω).

In a typical Doppler Free Spectroscopy set up, a beam splitter is used to divert a small part of the probe beam to a photo receiver, which has two photo diodes, to serve as the reference beam with intensity I_R. The probe beam, after passing through the iodine cell, is also directed to one of the two photo diodes. Recalling the Lambert-Beer's law and Eqn. 2.1.2, the intensity of the probe beam after passing through the cell I_{probe} is given by

$$I_{probe}(\omega) = I_0 \exp(-\alpha(\omega)x) \simeq I_0(1 - \alpha(\omega)x) \tag{2.4.1}$$

The above taylor expansion assumes $\alpha(\omega)x$ is small. Now, if we balance both the reference and the probe beams such that they both share the same initial intensity I_0, we can measure $\alpha(\omega)$ through the following formula:

$$\alpha(\omega) = \frac{I_R - I_{Probe}}{I_R x} \tag{2.4.2}$$

A derivative of $\alpha(\omega)$ with respect to ω is then

$$\frac{\mathrm{d}\alpha}{\mathrm{d}\omega} = \frac{-1}{I_R x}\frac{\mathrm{d}I_{probe}}{\mathrm{d}\omega} \tag{2.4.3}$$

Because the pump beam was frequency modulated using the AOM, the frequency varies as follows:

$$\omega_{probe}(t) = \omega_0 + \omega_{bw}\sin\omega_{FM}t \tag{2.4.4}$$

where ω_{bw} is the modulation bandwidth and ω_{FM} is the modulation frequency. Taylor expanding $I_{probe}(\omega + \omega_{bw}\sin\omega_{FM}t)$ yields,

$$I_{probe}(\omega) = I_{probe}(\omega_0) + \sum_{n=1}^{\infty}\frac{\omega_{bw}^n}{n!}\sin^n\omega_{FM}t\left[\frac{\mathrm{d}^n I_{probe}}{\mathrm{d}\omega^n}\right]_{\omega=\omega_0} \tag{2.4.5}$$

Combining Eqn. 2.4.5, Eqn. 2.4.3 and 2.4.2, we obtain [5]

$$\alpha(\omega) = -\sum_{n=1}^{\infty}\frac{\omega_{bw}^n}{n!}\sin^n\omega_{FM}t\left[\frac{\mathrm{d}^n\alpha}{\mathrm{d}\omega^n}\right]_{\omega=\omega_0} \tag{2.4.6}$$

Eqn. 2.4.6 can be further rewritten as[5]:

$$\begin{aligned}
\alpha(\omega) = &\left(\frac{\omega_{bw}^2}{4}\left[\frac{\mathrm{d}^2\alpha}{\mathrm{d}\omega^2}\right]_{\omega=\omega_0} + \frac{\omega_{bw}^4}{64}\left[\frac{\mathrm{d}^4\alpha}{\mathrm{d}\omega^4}\right]_{\omega=\omega_0} + \cdots\right)\\
&+\left(\frac{\omega_{bw}}{1}\left[\frac{\mathrm{d}\alpha}{\mathrm{d}\omega}\right]_{\omega=\omega_0} + \frac{\omega_{bw}^3}{8}\left[\frac{\mathrm{d}^3\alpha}{\mathrm{d}\omega^3}\right]_{\omega=\omega_0} + \cdots\right)\sin(\omega_{FM}t)\\
&+\left(-\frac{\omega_{bw}^2}{4}\left[\frac{\mathrm{d}^2\alpha}{\mathrm{d}\omega^2}\right]_{\omega\omega_0} + \frac{\omega_{bw}^4}{48}\left[\frac{\mathrm{d}^4\alpha}{\mathrm{d}\omega^4}\right]_{\omega=\omega_0} + \cdots\right)\cos(2\omega_{FM}t)\\
&+\left(-\frac{\omega_{bw}^3}{24}\left[\frac{\mathrm{d}^3\alpha}{\mathrm{d}\omega^3}\right]_{\omega=\omega_0} + \frac{\omega_{bw}^5}{384}\left[\frac{\mathrm{d}^5\alpha}{\mathrm{d}\omega^5}\right]_{\omega=\omega_0} + \cdots\right)\sin(3\omega_{FM}t)\\
&+\cdots
\end{aligned} \tag{2.4.7}$$

If the modulation bandwidth is small and $\omega_{bw}/\omega_0 \ll 1$, we only need to consider the first order terms in each of the coefficients of $\sin((2m+1)\omega_{FM}t)$ and $\cos((2m)\omega_{FM}t)$, where m is a positive integer, while the consecutive terms can be

ignored. Next, we pass the above signal into the Lock-in Amplifier. We use a sinusoidal reference signal with frequency ω_{FM}. passing the signal through the mixer, we obtain the $S_{mixed}(\omega)$

$$\begin{aligned} S_{mixed}(\omega) &\simeq \sin(\omega_{FM})\alpha(\omega) \\ &= \left(\omega_{bw}\left[\frac{\mathrm{d}\alpha}{\mathrm{d}\omega}\right]_{\omega=\omega_0}\right)\sin^2(\omega_{FM}t) + \cdots \\ &= \omega_{bw}\left[\frac{\mathrm{d}\alpha}{\mathrm{d}\omega}\right]_{\omega=\omega_0}\frac{1}{2}\left(1-\cos(2\omega_{FM}t)\right) \end{aligned} \tag{2.4.8}$$

The other terms can be ignored because when we pass $S(\omega)$ through the low pass filter, the high frequency components will be filtered out. Note also the DC term in Eqn. 2.4.8 which will be the only term that survives after passing the signal through the low-pass filter. Hence,

$$\begin{aligned} S(\omega) &= \frac{1}{nT}\int_0^{nT}\omega_{bw}\left[\frac{\mathrm{d}\alpha}{\mathrm{d}\omega}\right]_{\omega=\omega_0}\cos(2\omega_{FM}t) \\ &= \frac{\omega_{bw}}{2}\left[\frac{\mathrm{d}\alpha}{\mathrm{d}\omega}\right]_{\omega=\omega_0} \end{aligned} \tag{2.4.9}$$

Notice that the magnitude of $S(\omega)$ is proportional to the modulation bandwidth. Our lock-in signal is a derivative of the doppler free peaks. Hence, since the doppler free peak is a Lorentzian, the derivative of the Lorentzian is

$$\begin{aligned} \frac{\mathrm{d}\alpha}{\mathrm{d}\omega} &= \frac{\mathrm{d}}{\mathrm{d}\omega}\left[\frac{A\gamma_0/2\pi}{(\omega-\omega_0)^2+(\gamma_0/2)^2}\right] \\ &= \frac{2A\gamma_0/2\pi(\omega-\omega_0)}{((\omega-\omega_0)^2+(\gamma_0/2)^2)^2} \end{aligned} \tag{2.4.10}$$

With maxima/minima at

$$\omega = \omega_0 \pm \frac{\gamma}{2\sqrt{3}} \tag{2.4.11}$$

and amplitude difference between the maxima and minima is

$$\Delta\alpha' = \frac{3\sqrt{(3)}A}{\gamma^2} \tag{2.4.12}$$

Of particular note, would be that measuring the frequency difference between the maxima and minima would yield a value proportional to linewidth of the Lorentzian and measuring the amplitude difference between the two maxima and minima would yield a value proportional to the amplitude of the Lorentzian. Both quantities are useful when we are determining the doppler linewidth and the absolute intensity of the signal. An example of a lock signal is depicted in Fig.2.6.

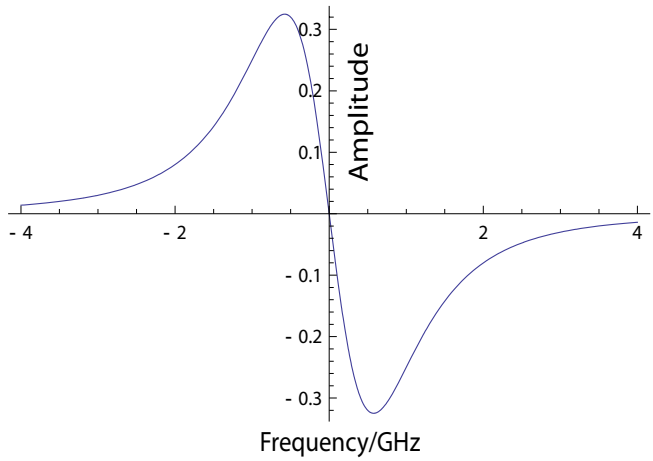

Figure 2.6: Lock Signal. Notice that it is a derivative a Lorentzian.

2.5 Optimizing the Signal

Since the lock-in signal depends on the amount of absorption that takes place as the laser travels through the cell, we need to optimize the beam profile to maximize the lock-in signal especially when the laser power sent to lock is typically about 25mW. To optimize the signal, we need to find the ideal waist of the laser beam to maximize the interaction between the laser beam and the Iodine molecules.

Let us first consider the intensity profile of the laser beam. The intensity profile of a TE_{00} single mode Gaussian beam defined as follows:

$$I(r,z) = \frac{2P}{\pi\omega_0^2} e^{-\frac{2r^2}{w(z)^2}} \tag{2.5.1}$$

where $w(z)$ is the beam radius as a function of distance z from the point of emission and is also the FWHM of the Gaussian beam.

$$w(z) = w_0\sqrt{1 + \left(\frac{z}{z_R}\right)^2} \tag{2.5.2}$$

where Rayleigh's range z_R for the beam is given by

$$z_R = \frac{\pi w_0^2}{\lambda} \tag{2.5.3}$$

and w_0 is the beam waist at the narrowest point and λ here is the wavelength of the laser beam. The Rayleigh range is regarded as the distance between the between point where the the Gaussian Beam has waist $\sqrt{2}w_0$ and w_0. The Rayleigh range is thus the spatial region where the molecules would interact most with the laser as the laser intensity is at its highest. Hence, it is important that most of the Iodine cell is placed within the Rayleigh range of both laser beams to ensure maximum interaction between the laser beam and the iodine molecules in the cell.

The intensity of the probe beam, which it is assumed to be a TE_{00} single mode Gaussian beam, as it passes through the iodine cell is a combination of Eqn. 2.5.1 and Eqn.2.1.2 as a result of the Lambert-Beer law. The equation is given to be:

$$I_{probe}(r, z) = \epsilon\frac{2P}{\pi\omega_0^2}e^{-\rho_a\sigma_{opt}z - \frac{2r^2}{\omega(z)^2}} \tag{2.5.4}$$

where ϵ is the fraction of the pump beam power and σ_{opt} is the transition cross-section at resonance and it is defined as

$$\sigma_{opt} = \frac{3\lambda^2}{2\pi} \tag{2.5.5}$$

and the actual number density ρ_a accessible to the laser is a function of ρ_0 which is the number density of the molecules accessible to the laser and ρ_0 is given by

$$\rho_0 = pn\frac{\gamma_0}{\gamma_D} \tag{2.5.6}$$

where p is the probability of a transition, and γ_0 and γ_D are the natural linewidth and doppler linewidth (Eqn.2.2.8) as before. n is the number density of molecules in the cell, and is defined as according to the ideal gas law:

$$n = \frac{P}{kT} \tag{2.5.7}$$

where P is the iodine cell pressure at room temperature, and T is the cell temperature and k is the Boltzmann constant. To determine actual number density ρ_a, we must determine the fraction of the population available for interaction with the probe beam after saturation by the pump beam. Assume that Iodine is a two level system and that our laser beams are locked tightly to the resonance frequency of 739nm. The population of molecules in the excited state ρ_{ee} (Eqn.2.2.18) becomes

$$\rho_{ee} = \frac{s_0}{1 + s_0} \tag{2.5.8}$$

Since the population of molecules in the ground state is given by $\rho_{gg} = 1 - \rho_{ee}$, and that the actual density of molecules ρ_a that can interact with the probe beam when the pump beam is shone through is proportional to $\rho_{ee} - \rho_{gg}$ so

$$\rho_a = \rho_0 \left(1 - \frac{s_0}{1 + s_0}\right) = \rho_0 \delta_{rho} \tag{2.5.9}$$

where δ_{rho} is paremeter defined as $\delta_{rho} = \left(1 - \frac{s_0}{1+s_0}\right)$. Since $s_0 = I/I_s$, for simplicity, take I to be the average intensity of the laser beam, which is given to be $I = \frac{P}{\pi\omega^2}$ so that we do not have to worry about spatial dependency. Hence, the intensity of the probe beam in the presence of a pump beam which saturates the cell is given by

$$I^p_{probe} = I_0 e^{-\rho_0 \sigma_{opt} \delta_{rho} z - \frac{2r^2}{\omega(z)^2}} \tag{2.5.10}$$

Without the pump beam, only the probe beam will be interacting with the molecules, of which most have not been excited to the excited state and hence the more of the

probe beam will be absorbed. Thus, the intensity is given by

$$I_{probe}^{n.p.} = I_0 e^{-\rho_0 \sigma_{opt} z - \frac{2r^2}{\omega(z)^2}} \tag{2.5.11}$$

To obtain an equation which maximizes the signal, we will integrate $\Delta I = I_{probe}^{p} - I_{probe}^{n.p.}$ over a cylinder of length $2z_R$ but infinite width since this is the region when the laser is most intense and thus the greatest amount of interaction between the probe beam and Iodine molecules will take place here and produce the most signal. Thus we have

$$\begin{aligned} \Delta I &= \int_{Vol} \left(I_{probe}^{p} - I_{probe}^{n.p} \right) \mathrm{d}V \\ &= \epsilon \frac{2P}{\pi w_0^2} \int_0^{\infty} e^{\frac{2r^2}{w_0^2}} \int_0^{2z_R} \left(e^{-\rho_0 \sigma_{opt} \delta_{rho} z} - e^{-\rho_0 \sigma_{opt} z} \right) \mathrm{d}z 2\pi r \mathrm{d}r \end{aligned} \tag{2.5.12}$$

$$\Delta I = \epsilon \frac{2P}{\pi w_0^2} 2\pi \frac{\omega^2}{4} \left(\frac{-e^{-2\rho_0 \sigma_{opt} w z_R} + 1}{\rho_0 \sigma_{opt} w} - \frac{e^{-2\rho_0 \sigma_{opt} z_R} - 1}{\rho_0 \sigma_{opt}} \right) \tag{2.5.13}$$

The difference in intensity ΔI is a function of the beam waist w_0. By plotting ΔI versus w_0 and finding the maxima of the equation, we are able to determine which value of w_0 gives us the best signal required for the lock.

Now, we may calculate the best possible laser waist that optimizes our pump-probe signal. Table 2.1 lists down the values of the variables to be used for our model. To estimate the vapor pressure of Iodine, the vapor pressure of crystalline

Table 2.1: Variables and Constants

Variable/Constant Name	Value
Mass of Iodine Molecule m	4.21322×10^{-25} kg
fraction of pump beam power ϵ	0.1
Pump Beam Power P	.02mW
Laser/Iodine Spectrum Wavelength λ	739nm
Approximate Life Time τ	10^{-6} s

Iodine varies according to this table [20]: Using the above values the log of the vapor pressure P with base 10 was plotted against temperature T in Fig. 2.7 Igor was use

Table 2.2: Iodine vs Temperature[20]

Temperature / K	260	282	309	342	381	457
Pressure / Pa	1	10	10^2	10^3	10^4	10^5

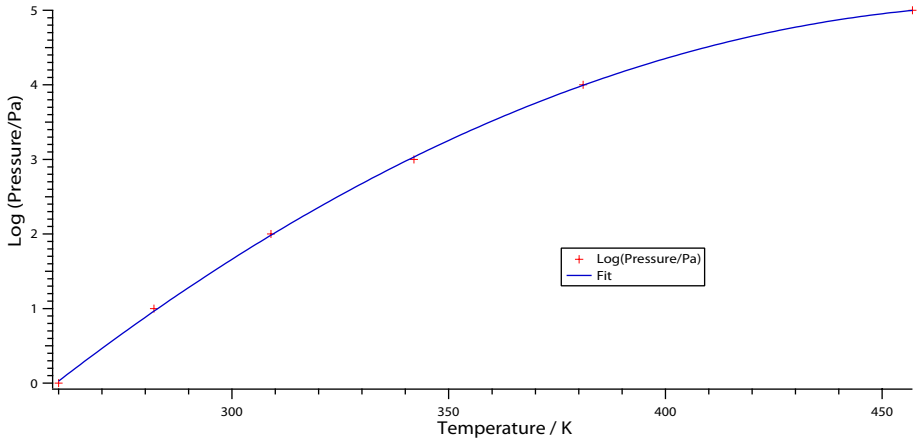

Figure 2.7: log Pressure/Pa vs Temperature/K. The polynomial fit of the curve was done using Igor to estimate the variation of Pressure vs Temperaure

to fit the data in Fig. 2.7, yielding the fit equation:

$$\log_{10} P = -18.339 + 0.096468T - 9.9349 \times 10^{-5}T^2 \tag{2.5.14}$$

The estimated pressure at room temperature 293 K was found to be 24.9 Pa. With all the necessary parameters, we plot the ΔI in Fig. 2.8. The best beam waist we need for our experiment is approximately $200\mu m$ according to Fig. 2.8

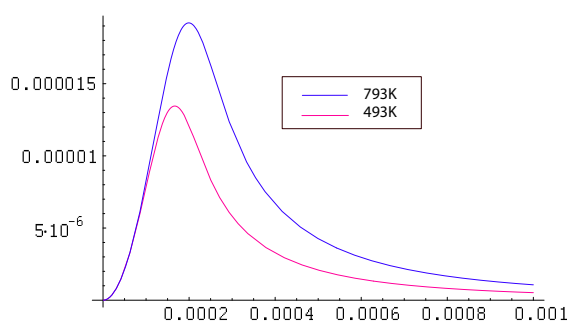

Figure 2.8: Δ I vs Beam Waist/m. The maxima of the curves gives us the optimum beam waist required for our experiment. The best beam waist is approximately $200\mu m$.

CHAPTER III

Experimental Setup

In this chapter, we will describe the experimental setup and briefly introduce the important techniques and equipment used in the setup and finally how we would optimize our signal.

3.1 Optics Setup

The relevant optics and electronics required for the proposed Pound-Drever-Hall laser lock [6, 1] are shown in Fig.3.1 and is similar to what was done in the Ytterbium Ion-Photon entanglement experiment [27, 25, 22]. 0.5 mW of laser power is sent from the diode laser through a half waveplate and a polarizing beam splitter (PBS) into a single-mode optical fiber which directs the 25 mW of power to the Iodine lock. Note that for the purpose of spectroscopy, we will be directing more power to the iodine lock so as to take data required to analyze the iodine spectrum. We will replace this optical fiber with a fiber electro-optical modulator (EOM), so that we can change the frequency offset point for our laser frequency stabilization. The advantage of using an optical fiber is that the optical fiber acts as a spatial filter and produces a single mode TE_{00} beam. In our experiment, we have coupled more than 50%.

The signal from the lock is then directed to a proportional integral derivative servo controller (PID). 2 mW of the main beam is sent to a reference invar cavity

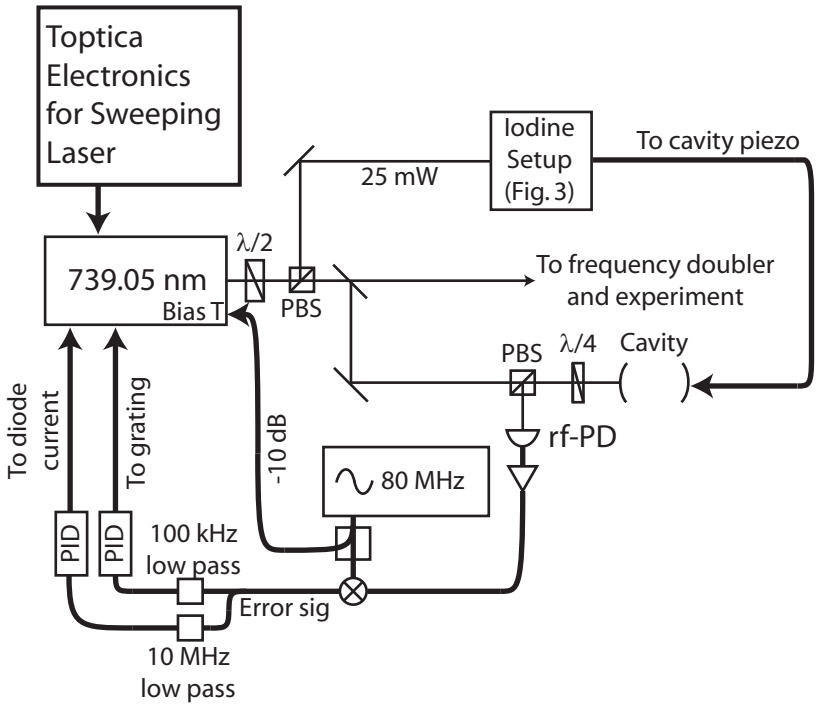

Figure 3.1: 739nm Laser Lock. 0.5 mW of laser power is sent from the diode laser through a half waveplate and a polarizing beam splitter (PBS) into an optical fiber which directs the 25 mW of power to the Iodine lock. Note that for the purpose of spectroscopy, we will be directing more power to the iodine lock so as to take data required to analyze the iodine spectrum. The signal from the lock is then directed to a proportional integral derivative servo controller (PID). Because the signal from the lock is typically too weak, 2 mW of the main beam is sent to a reference invar cavity with a cavity piezo controlled by the aforementioned PID. Essentially this cavity is stabilized by the iodine lock. Invar is used to ensure maximum thermal stability. The output from the cavity is measured by a radio-frequency photodiode (PD) and the signal is then amplified by an amplifier and mixed a 120MHz signal modulating the Bias T of the laser. The signal from the radio-frequency photodiode is subsequently routed through 2 low pass filters followed by PIDs to control the laser diode current and laser grating, thus stabilizing the frequency of the laser.

with a cavity piezo controlled by the aforementioned PID. Essentially this cavity is stabilized by the iodine lock. Invar is used to ensure maximum thermal stability. The output from the cavity is measured by a radio-frequency photodiode (PD) and the signal is then amplified by an amplifier and mixed a 120MHz signal modulating the Bias T of the laser. The signal from the radio-frequency photodiode is subsequently routed through 2 low pass filters followed by PIDs to control the laser diode current and laser grating, thus stabilizing the frequency of the laser.

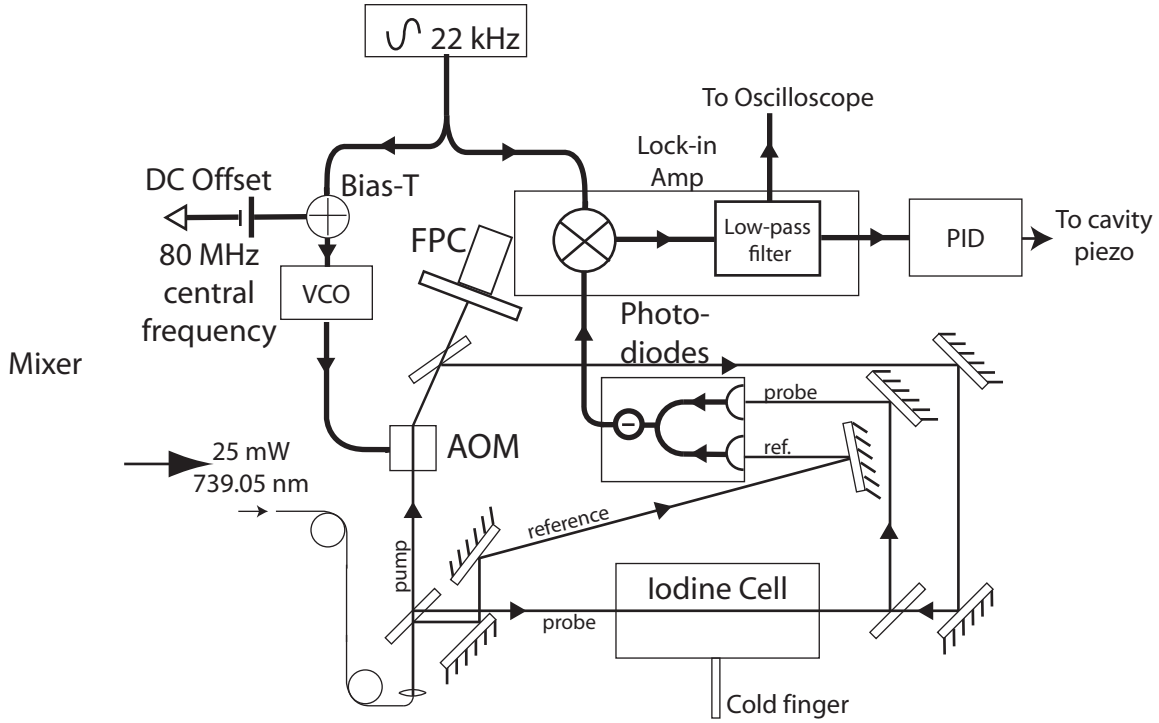

Figure 3.2: The laser beam from the optical fiber is then split between the pump and probe beam with about > 1% power diverted to the probe beam. The pump beam goes through an AOM and the 1st order is selected. Another small part of the probe beam is diverted with a beam splitter to the photo receiver as the reference beam. Both the reference and probe beams are focused tightly with two 10 cm lens. Both the pump and probe beam have an approximately 9:1 ratio in terms of power and are focused into the Iodine cell with 20cm lens. The two lens are 43cm apart so that the Rayleigh range of both the probe and pump beam overlap as much as possible. For the purpose of measuring the iodine spectrum, we will send the output signal from the lock-in amplifier and the doppler signal from the photodiode to the oscilloscope. Note also the Fabry Perot Cavity (FPC) that we use to check whether the laser mode is clean.

The laser beam from the optical fiber is then split between the pump and probe beam and reference beam using a beam splitter with about > 1% power diverted to the probe beam. The pump beam goes through an AOM and the 1st order is selected. Using a beam splitter, a small part of the pump beam is diverted to a Fabry-Perot Cavity (FPC) to allow us to check that the laser is single mode. Both the reference and probe beams are focused tightly with two 10cm lens. Both the pump and probe beam have an approximately 9:1 ratio in terms of power and are focused into the Iodine cell with 20cm lens. The beam radius at the focus of the two

lens was measured using a beam profiler and found to be 100μm. The two lens are 43cm apart so that the Rayleigh range of both beams overlap as much as possible.

For the purpose of the measuring the iodine spectrum, we will sweep the 739nm laser using the Toptica electronics supplied with the laser. The trigger from the sweep and the output signal from the photodiode and the lock-in amplifier from the iodine setup is sent to the oscilloscope to allow us to collect data. The power sent to the iodine setup instead can be up to 100mW depending on the measurements we would like to take.

3.2 Iodine Cell

The iodine cell is a glass cell with tapered quartz windows and a cold finger that is kept at room temperature. The quartz windows are tapered at Bragg angle, hence any beam that enters parallel to the axis of the cell enters at Bragg angle and the reflected beam is polarized. It is 30cm long, and 0.5" wide. The cell was manufactured by a commercial company whereby iodine was pumped and evaporated at 50°C until no more iodine could be evaporated. To reduce radiation of heat, the cell is wrapped around with many layers of aluminium foil and fiber glass. The cell is first surrounded by layers of aluminium before the heating tape (FGS051-020 fiber glass insulated heater tape by Omega Engineering Inc.) is wrapped around the cell. This ensures even heating of the cell and prevent any fractures due to uneven heating. A J-type thermocouple (XC-24-J-12 thermocouple by Omega Engineering Inc.) which is capable of measuring temperature up to 700°C is inserted after the heating tape is also wrapped around with more layers of aluminium. As stated in the previous chapter, the iodine cell was heated to approximately 500°C. It must be carefully heated to ensure it does not fracture due to rapid expansion or contraction.

Two aluminium plates are placed at each end of the cell to reflect the heat back to the cell window and prevent the heat from affecting the surrounding optics. The plates have holes to allow the counterpropagating pump and probe beams to pass through.

The cold finger is approximately 15cm long and is coated with thermal paste to allow easy conduction of heat to the copper mesh that is wrapped around it. The copper mesh serves as a heat sink to conduct heat away from the cold finger. A thermocouple is also inserted in the copper mesh to allow us to monitor the temperature of the cold finger. The cold finger is typically kept in the temperatures from $28°C - 32°C$. The temperature of the cold finger is small compared to the cell temperature, which is typically greater than $200°C$. One way to understand how the cell works is to note that there is a pressure difference between the cold finger and the cell due to the large difference in temperatures between the cold finger and the cell. As a result, iodine molecules are pushed into the cold finger where it condenses at near room temperature. As a result, the population of iodine molecules in the cell decreases and maintain the vapour pressure of the cell at room temperature and thus reduces the probability of collisions between atoms responsible for pressure broadening. One would think that the reduction in population of molecules would affect the signal. On the contrary, the high temperature would populate more molecules in the upper vibrational levels in the ground manifold as mentioned in the last chapter and increase the optical density at the 739nm.

3.3 AOM

The AOM or Acoustic Optical Modulator, modulates the pump laser by adding a frequency offset and adding a sinusoidal modulation to the laser. It does this by

Figure 3.3: Iodine Cell without Insulation. Here we have the iodine cell wrapped with only heater tape and aluminium foil. The heater tape is wrapped such that heat is evenly distributed across the cell.

using an acoustic wave produced by a piezo-electric transducer that vibrates at the supplied frequency that changes the structure of the crystal to form a moving bragg grating. The angle of diffraction follows this relation[30]:

$$\sin\theta = \frac{m\lambda}{2\lambda_s}, m = 0, \pm 1, \pm 2, ... \tag{3.3.1}$$

where λ and λ_s are the wavelength of the laser and sound wave and m is the order. The moving wave also gives a momentum kick to the laser beam and such that the frequency f is given by $f' = f + mF$ where F is the frequency of the sound wave and m is the order of diffraction. The AOM is given a central frequency of 80MHz by a Voltage Controlled Oscillator(VCO) and 22KHz modulation provided by a signal generator.

3.4 Photoreceiver and Lock in Amplifier

The photoreceiver receives the reference beam and the probe beam and subtracts the reference beam from the probe beam. Both beams should be balanced in intensity

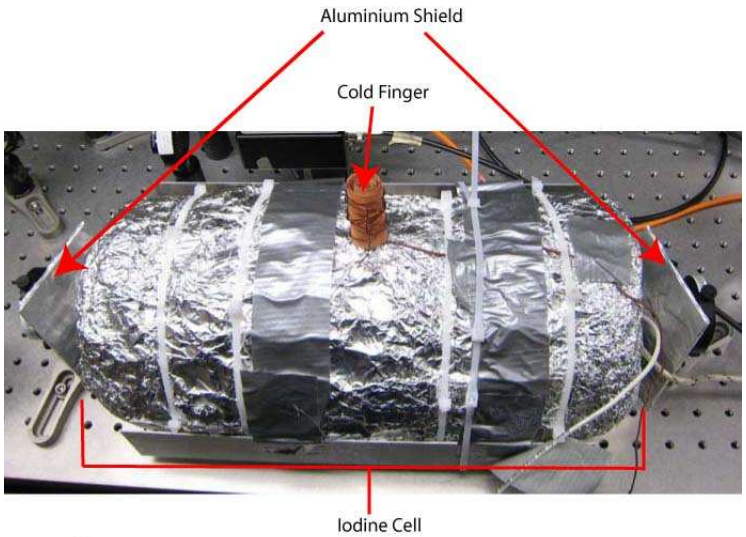

Figure 3.4: The cell is wrapped with many layers of aluminium and fiber glass to insulate the cell. A heater tape is wrapped round the cell after the initial few layers of aluminium to ensure even heating of the cell. J-type thermocouple inserted after a few layers of aluminium around the heater tape. The cold finger is coated with thermal paste to allow easy conduction of heat to the copper mesh wrapped around it. The copper mesh serves as a heat sink to conduct heat away from the cold finger. A thermocouple is also inserted in the copper mesh to allow us to monitor the temperature of the cold finger.

to cancel the Direct Current (DC) background and the common mode noise, such as laser power fluctuations. Subtraction of the DC background also reserves the dynamic range of the amplifier gain for the error signal.

As mentioned in section 2.4, the Lock-in Amplifier is a demodulator. A 22KHz signal (same as the one sent to the AOM) is sent to the Lock-in Amplifier whereby the mixer multiplies the 22KHz signal with the error signal and the low pass filter filters out the high frequency components. The Lock-in amplifier then produces the derivative of the error signal from the photoreceiver. This derivative will be useful in allowing us to quantify the linewidth and the amplitude of the absorption profile.

CHAPTER IV

Experimental Results

In this chapter, I will detail the experimental results obtained from the doppler free spectroscopy experiment. We explored the relation between signal strength and the temperature of the cell, doppler broadening and broadening effects.

4.1 The Signal at 739.0289

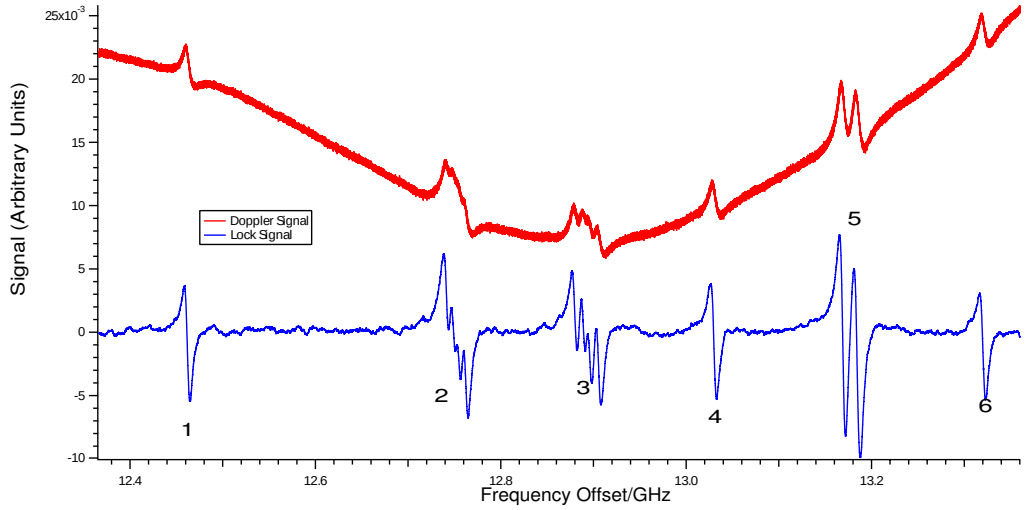

Figure 4.1: Doppler Signal and Lock Signal at $520°C$ showing the Hyperfine structure of Iodine. A total of 6 doppler free features are marked 1 - 6 here. The positive frequency offset is from 739.05204nm. Notice how the doppler free peaks in the doppler profile overlaps with the lorentzian derivatives in the lock signal.

To obtain extremely accurate measurements, the ratio between pump beam and the probe beam power has to be increased and the pump beam power kept as small

as possible. This is to minimize any power broadening of the signal. With 44mW for a pump beam and a 320μW probe beam, we obtain the following doppler broadened signal and lock signal in Fig. 4.1. The frequency scale in the figure is based on iodine spectroscopy data obtained by Steven Olmschenk et. al [27]. In the figure, we labeled 6 features from 1 to 6 with error of $\pm 0.1GHz$, centered at 739.0297nm, 739.0292nm, 739.0289nm, 739.0287nm, 739.0284nm and 739.0282nm respectively, with error of $\pm$0.01GHz to account for laser drifting. The signal has a similar pattern to the lines at 739.034 nm [27] and to the lines at 657 nm [26] which might imply that the transitions at 739.0289 nm are similar to the transitions that results in the P(84) line in the 5-5 band at 657nm. This ratio of pump beam to the probe beam is not the atypical ratio we would use in the main experiment as the probe beam would be otherwise far too weak when only 5mW of power is delivered to the setup. Some 100mW of laser power was delivered to the setup with the use of optics filters to reduce the intensity of the pump beam.

Notice in Fig. 4.1, signal feature 1, 4 and 6 are clear and distinct with no hyperfine structure, while 2, 3, and 5 have hyperfine structure in them. Also note that the doppler free peaks in the doppler signal overlaps with the lorentzian derivatives in the lock signal. Further, it's possible that feature 2 is the crossover signal for feature 1 and 4 since the middle between 1 and 4 is 739.0293nm, while feature 3 is a crossover signal for feature 1 and 6 since the mid point is 739.0289nm. Feature 5 is a crossover between 4 and 6 since the mid point is 739.0285nm. However, with the hyperfine structure in feature 2, 3 and 5 may mean they are either not crossover signals, or are superpositions of other signals. The linewidths of the features, in ascending order, are measured to be 0.02910GHz, 0.09041GHz, 0.11293GHz, 0.02425GHz, 0.093138GHz and 0.02078GHz with error of $\pm$0.01732GHz to account for noise and laser drifting.

4.2 Temperature and Signal Strength

To see how the signal strength varies according to temperature, we choose a number of data points and then heat the cell up to the required temperature and hold the temperature steady for several minutes to ensure thermal equilibrium was achieved. The spectrum and the lock-in signal is subsequently taken. We keep the cell from heating beyond $600°C$ to ensure that the cell does not expand too much and crack. We measure the peak the peak amplitude of one of the peaks in each of the lock-in signal versus temperature and plot the graph in Fig.4.2. The

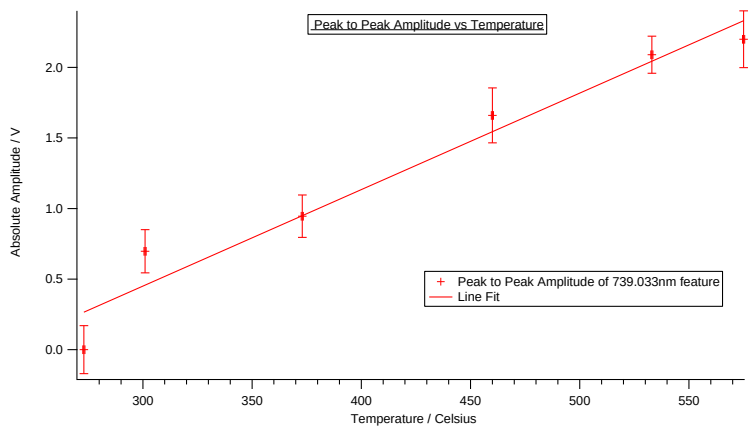

Figure 4.2: Peak to Peak Amplitude vs Temperature of feature 6. The signal increases in intensity as temperature rises. To ensure the best signal possible while keeping the temperature under $600°C$, we should keep the cell heated at $500°C$. The equation of the fit line is $y = -1.6008 \pm 0.315 + (0.006838 \pm 0.000727)x$

amplitude/Temperature gradient is 0.006838 ± 0.000727 mV/K. From the fit line, there should be negligible signal strength at temperatures less than 234 degrees Celsius, which is in line with what we saw in our experiments. It would appear that the best possible temperature for our lock is at $500°C$ which is more line with the expectation as noted in Tiemann et. al[19]. The ground states for the transitions must be sufficiently populated to provide us with substantial signal. The test was done with a ratio 1 : 10 of 1mW probe power to 10mW of pump power.

4.3 Doppler Broadening

Measuring the doppler Broadening is difficult as the peaks are very close to each other and thus it is hard to measure the doppler linewidth. What we tried to do instead is to fit the signal to a sum of 6 Gaussian curves with the appropriate center frequencies. In addition, we added a weightage a_i of each curve as many of the peaks are very close to each other and as a result, certain features in the lock-in signal are actually a sum of a number of peaks. The normalized weightage is determined by multiplying a weightage to each amplitude of each doppler peak and then divided by the total sum of weighted amplitudes. The formula of the fit is given to be:

$$I_{fit} = y_0 + A \sum_{i=1}^{6} a_i e^{\frac{(\omega-\omega_i)^2}{(\omega_D(T))^2}} \tag{4.3.1}$$

where $a_1 = 0.07029$, $a_2 = 0.3183$, $a_3 = 0.2569$, $a_4 = 0.06829$, $a_5 = 0.2192232$, $a_6 = 0.06696347$ and $\omega_D(T)$ is the doppler linewidth as defined by Eqn. 2.2.8. ω_i is the center frequency of the 6 features as was mentioned in section 4.1. A and y_0 are fit variables to be determined by the fitting algorithms. Igor Pro 5.0 was used to do the fits and calculate the χ^2 value for the curves to see the goodness of fit. The fits are shown in Fig. 4.3, 4.4 and 4.5

A χ^2 goodness of fit test with degree of freedom n = 9994 will indicate how good our fit is. The reduced χ^2/n for each fit is less than one. This might indicate that the doppler broadening equation is correct.As we note, the fits in Fig. 4.3 to Fig. 4.5 appear to match the recorded spectrum which may indicate that the fit function is correct. One might even note that at low temperature, one starts to see some distinct evidence of the multiple Gaussian absorption profiles.

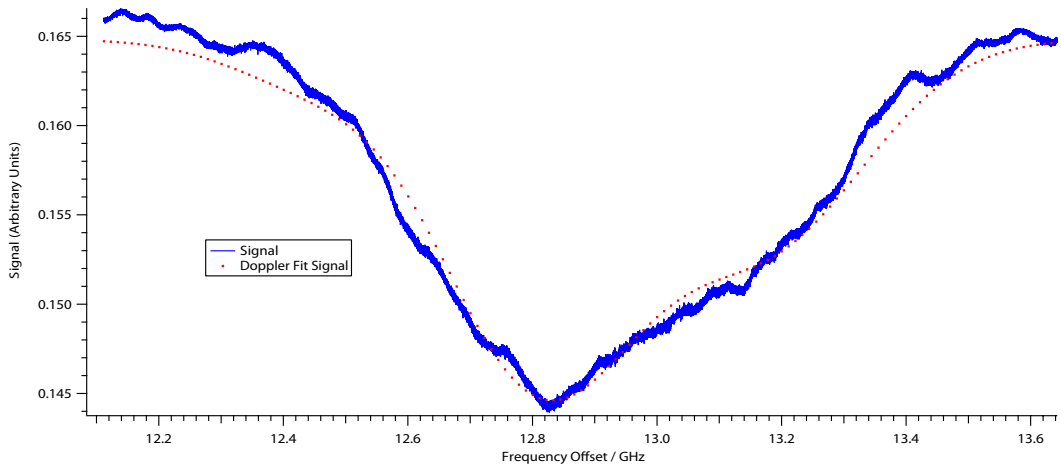

Figure 4.3: Doppler fit of Doppler Signal at $301°C$. $\chi^2 = 3.05901$ The fit is clearly not very good. One might however note that the profile is not as smooth as the plots at higher temperatures, giving hint to the multiple absorption profiles.

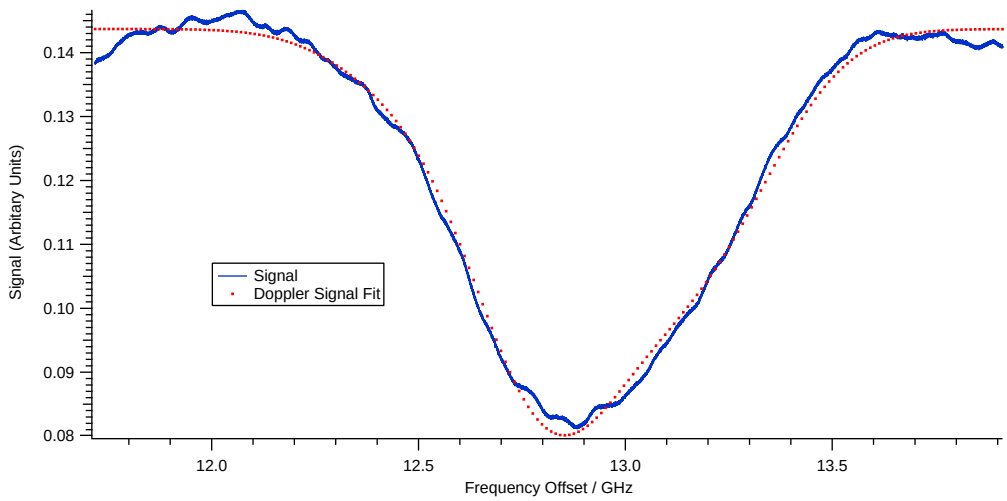

Figure 4.4: Doppler fit of Doppler Signal at $460°C$. $\chi^2 = 0.285219$ The model is a good fit for the signal.

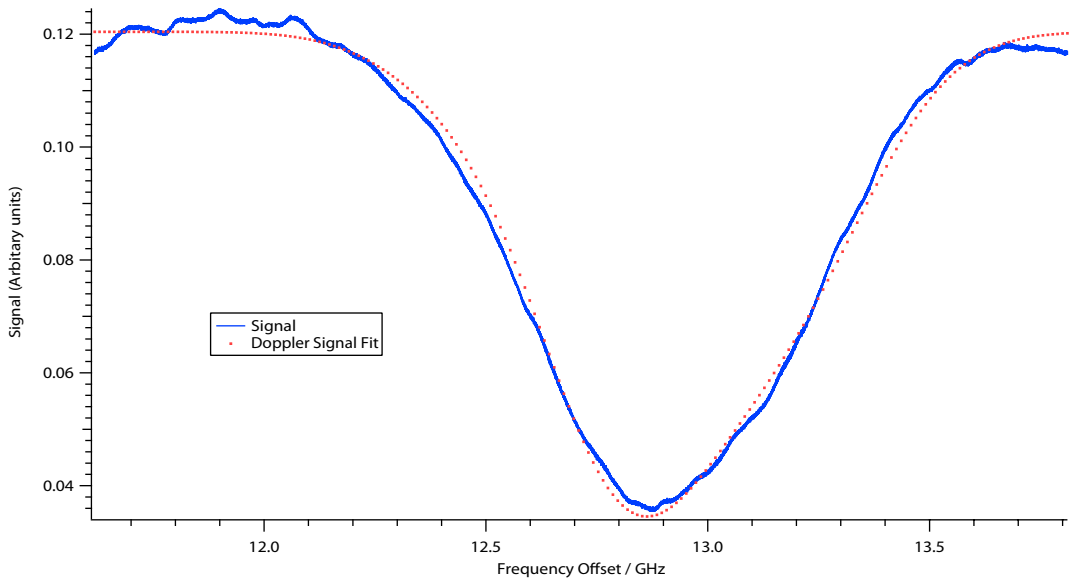

Figure 4.5: Doppler fit of Doppler Signal at $533°C$. $\chi^2 = 0.440139$ The model is a good fit for the signal.

4.4 Power Broadening

To measure power broadening, we maintain the probe beam at a constant power of $320\mu W$ and vary the power of the pump beam. This is to keep any power broadening by the probe beam to the very minimum. Since the absolute intensity of the signal is expected to be proportional to the light scattered from the population in the excited state γ_s (Eqn.2.2.21) and that the saturation intensity I_s is intensity of the laser beam at half the maximum possible scattering rate, our fit function for our data is of the form:

$$\gamma_{s,fit} = A' \frac{x/B'}{1 + x/B'} \tag{4.4.1}$$

where A' and B' are fit parameters, and B' is the saturation intensity I_s. Choosing feature 1, 4 and 6 in the lock signal, we plot the graph of absolute intensity of the signal versus power of the pump beam in Fig. 4.6, 4.7 and 4.8.

From the fit in the Fig.4.6, 4.7 and 4.8, saturation intensity I_s has values $I_s =$ 7.5136 ±0.73mW, 7.5134 ±0.68mW and 7.4368 ±0.68mW respectively. To calculate

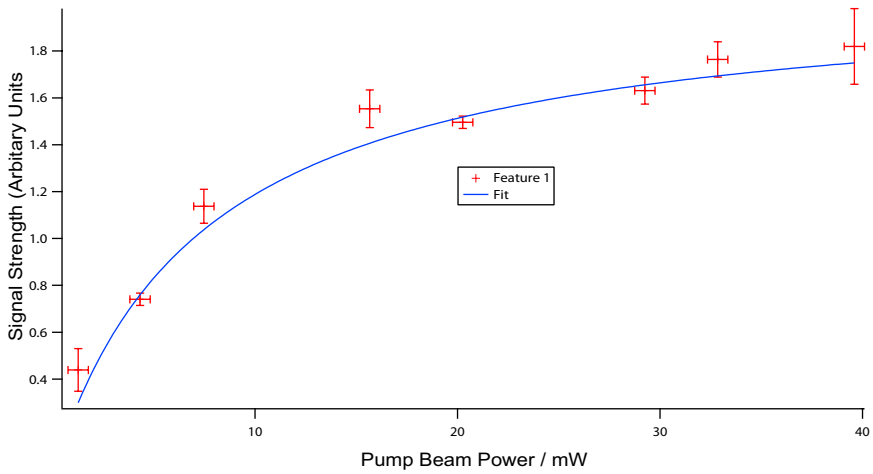

Figure 4.6: Signal Peak to Peak amplitude vs Power of Pump beam for Feature 1. The fit has parameters A' = 1.9223 and B' = 7.5136 This implies that the saturation intensity is I_s = 7.5134 ±0.73mW. The saturation intensity per unit area for a 100μm is 23915 ±2355 mW/cm^2. Error bars for Power was approximately $\pm 0.5mW$ to account for random fluctuations in power and error bars for intensity is based on the noise signal strength.

the saturation intensity, we first measured the waist of the beam at the focus of the lens using a CCD (Charge Coupled Device) camera and the beam waist was 100μm. The saturation intensities for a 100μm beam waist is 2.39±0.23 W/cm^2, 2.39±0.21 W/cm^2 and 2.36 ±0.21W/cm^2 respectively. This suggest a saturation intensity per unit area of 2.38 W/cm^2. This saturation intensity is rather high but it is expected given that the Iodine molecule has a complicated energy level structure.

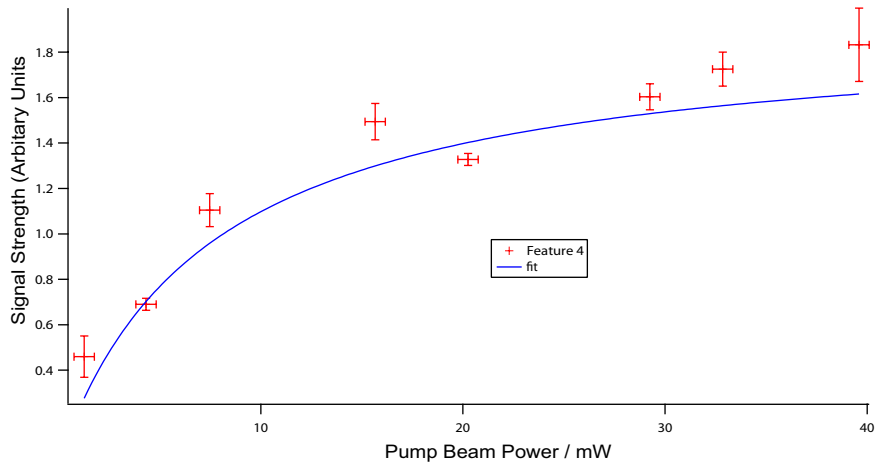

Figure 4.7: Signal Peak to Peak amplitude vs Power of Pump beam for Feature 4. The fit has parameters A' = 2.0811 and B' = 7.5134 This implies that the saturation intensity is I_s = 7.5136 ±0.68mW. The saturation intensity per unit area for a 100μm is 23915 ±2164 mW/cm^2. Error bars for Power was approximately $\pm 0.5mW$ to account for random fluctuations in power and error bars for intensity is based on the noise signal strength.

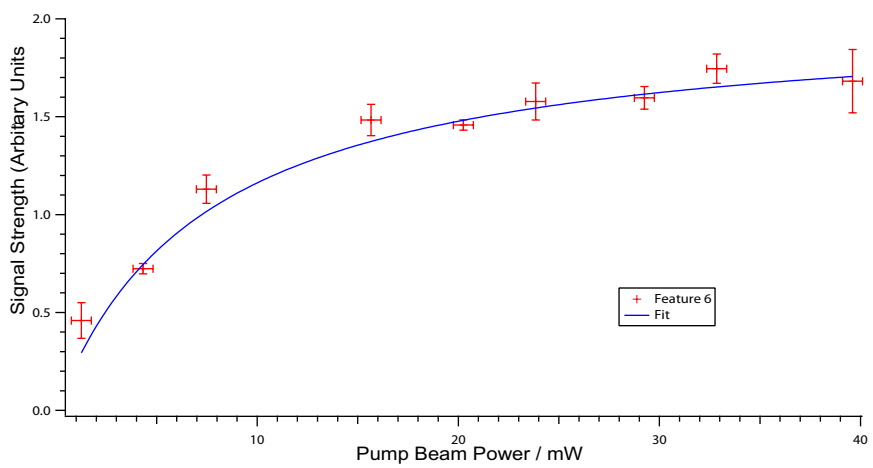

Figure 4.8: Signal Peak to Peak amplitude vs Power of Pump beam for Feature 6. The fit has parameters A' = 2.0258 and B' = 7.4368 This implies that the saturation intensity is I_s = 7.4368 ±0.68mW. The saturation intensity per unit area for a 100μm is 23672 ±2164 mW/cm^2. Error bars for Power was approximately $\pm 0.5mW$ to account for random fluctuations in power and error bars for intensity is based on the noise signal strength.

CHAPTER V

Future Development

No project is truly complete, and time constraints however, prevented some improvements to the setup to be implemented. Originally, it was planned to implement Multipass Doppler Free Spectroscopy instead to obtain a better doppler free spectrum. In this chapter, I will detail how the Multipass Spectroscopy is to be done, and how the setup could be optimized to produce the best possible doppler free spectrum.

5.1 MultiPass Spectroscopy

To further increase the signal strength of the doppler free spectrum, one might instead implement a multipass doppler free spectroscopy. The key difference is that instead of one single pass through the iodine cell, we place the iodine cell in the middle of a laser cavity. The key advantage to this system is that it increases the length of interaction between the laser and the iodine molecules and thus increase the amplitude of the doppler free signal. A way to reason this is to recall the Lambert-Beer's law and assume linear absorption. Let the length of interaction for the multipass spectroscopy is z_m and the length of the cell is z_{cell}. Thus $z_m > z_{cell}$ and from Lambert-Beer's law, the reduction in intensity due to linear absorption will thus be greater. A probe and pump beam again must be counterprogating, but both are aligned such that they enter the cavity at a small angle and thus reflect off the two

cavity mirrors repeatedly, passing through the cell many times before emerging from the cell. Extremely good mirrors are recommended, with power absorbed by the mirrors at most 1%.

This setup, as depicted in Fig. 5.1, is worth considering implementing especially when the lock-in signal gets weaker if less power is sent through an optical fiber EOM to the iodine lock setup, and locked to a FM sideband, leading to a reduction of the effective laser beam power. We may in the future implement the multipass configuration if the experiment demands it.

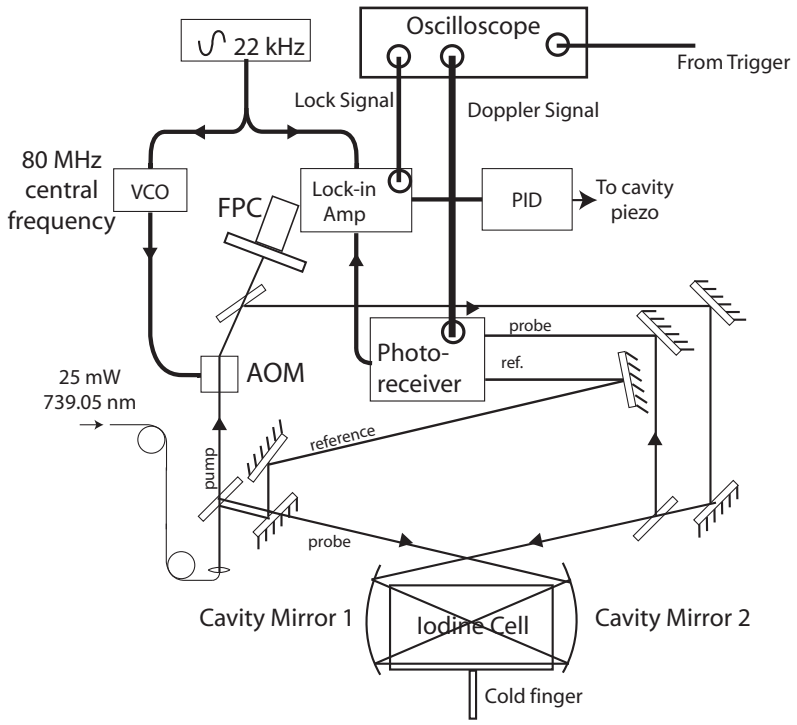

Figure 5.1: Multipass Spectroscopy. Here, the iodine cell is placed between two cavity mirrors and the probe and pump beam enter the cavity at a small angle to the horizontal. The two beams bounce back and forth between the two mirrors before emerging from the cell.

To optimize the signal, we should design our cavity such that the beam waist of the cavity mode matches what we had calculated in section 2.5. Then we should try to match our probe and pump beam waist to the beam waist of the cavity mode. However, the beams will enter the cavity at an angle, we should not expect the probe

and pump beam waist to completely match the cavity mode beam waist.

To calculate the beam waist ω_0 of the cavity mode, let us introduce two parameters known as the "resonator g parameters" g_1 and g_2

$$g_1 = 1 - \frac{L}{R_1} \tag{5.1.1a}$$

$$g_2 = 1 - \frac{L}{R_2} \tag{5.1.1b}$$

where L is the distance between the two cavity mirrors and R_1 and R_2 are the curvature of the two cavity mirrors used. The waist at the focus of the cavity mode is given by

$$w_0^2 = \frac{L\lambda}{\pi}\sqrt{\frac{g_1 g_1(1 - g_1 g_2)}{(g_1 + g_2 - 2g_1 g_2)^2}} \tag{5.1.2}$$

where λ is the wavelength of the laser. The spot size at the two mirrors are given by

$$w_1^2 = \frac{L\lambda}{\pi}\sqrt{\frac{g_1}{(g_1(1 - g_1 g_2)^2}} \tag{5.1.3a}$$

$$w_2^2 = \frac{L\lambda}{\pi}\sqrt{\frac{g_1}{(g_1(1 - g_1 g_2)^2}} \tag{5.1.3b}$$

In general, the parameters are kept within the stability range defined by [31]

$$0 \leq g_1 g_2 \leq 1 \tag{5.1.4}$$

In practice, symmetric confocal resonators are the simplest and most stable of resonators, with $g_1 = g_2 = 0$ and $R_1 = R_2 = L$. They are stable in that a slight misalignment will not change the beam focus spot size or position too much. However, we may not yield the correct beam focus waist w_0 and we are also limited by the available mirror curvature and also physical dimensions. Instead, we will go with

a symmetric resonator, with $g_1 = g_2 = g$ and $R_1 = R_2 = R$. Eqn. 5.1.2 and Eqn. 5.1.3 reduce to

$$w_0^2 = \frac{L\lambda}{\pi}\sqrt{\frac{1+g}{(4(1-g)}} \tag{5.1.5a}$$

$$w_1^2 = w_2^2 = \frac{L\lambda}{\pi}\sqrt{\frac{1}{1-g^2}} \tag{5.1.5b}$$

To determine the radius of curvature we need for our mirrors, we need to rearrange Eqn. 5.1.5. With a given w_0, define the parameter

$$\alpha = 4w_0^4\left(\frac{\pi}{L\lambda}\right)^2 \tag{5.1.6}$$

then g is

$$g = \frac{\alpha - 1}{\alpha + 1} \tag{5.1.7}$$

We then get the radius of curvature R, in terms of g, to be

$$R = \frac{L}{1-g} \tag{5.1.8}$$

With these equations, we can thus estimate the curvature of the mirror we would need, with a given distance L between the two mirrors and a given spot size w_0. For example, let L = 0.30m, and the wavelength λ will be 739nm, the corresponding waist would be 187.8 μm.

5.2 End Notes

In summary, doppler free spectroscopy of the Iodine molecule at 739nm was completed. The relationship between temperature and signal and the power broadening of the signal were examined, and the saturation intensity was found to be 2.38 W/cm^2. The setup was subsequently used to lock a 739nm laser.

BIBLIOGRAPHY

BIBLIOGRAPHY

[1] E. D. Black. An introduction to Pound-Drever-Hall laser frequency stabilization. *American Journal of Physics*, 69:79–87, January 2001.

[2] J. Cariou and P. Luc. Atlas du spectre d'absorption de la molecule d'iode 21100 cm^{-1} – 23800cm^{-1}. 1980.

[3] J. I. Cirac and P. Zoller. Quantum computations with cold trapped ions. *Phys. Rev. Lett.*, 74(20):4091–4094, May 1995.

[4] F. R. Petersen R. E. Drullinger K. M. Evenson D. A. Jennings, C. R. Pollock and H. P. Layer J. S. Wells, J. L. Hall. Direct frequency measurement of i_2-stabilized he-ne 473 thz (633nm) laser. *Optics Letters*, 8(3):136–138, 1983.

[5] W. Demoströder. *Laser Spectroscopy.* Springer-Veriag, 3rd edition, 2002.

[6] R. W. P. Drever, J. L. Hall, Hough J. Kowalski, F. V., G. M. Ford, A. J. Munley, and H. Ward. Laser phase and frequency stabilization using an optical resonator. *Appl. Phys. B: Photophys. Laser Chem.*, 31:97.

[7] C. S. Edwards, G. P. Barwood, P. Gill, F. Rodriguez-Llorente, and W. R. C. Rowley. Frequency-stabilised diode lasers in the visible region using doppler-free iodine spectra. *Opt. Commun.*, 132:94, 1996.

[8] R.P. Feynman. Simulating physics with computers. *Int'l J. Theo. Phys.*, 21, 1982.

[9] S. Gerstenkorn and P. Luc. Atlas du spectre d'absorption de la molecule d'iode 15600 cm^{-1} – 17600cm^{-1}. 1977.

[10] S. Gerstenkorn and P. Luc. Atlas du spectre d'absorption de la molecule d'iode 17500 cm^{-1} – 20000cm^{-1}. 1977.

[11] S. Gerstenkorn and P. Luc. Atlas du spectre d'absorption de la molecule d'iode 14000 cm^{-1} – 15600cm^{-1}. 1978.

[12] S. Gerstenkorn and P. Luc. Atlas du spectre d'absorption de la molecule d'iode 19700 cm^{-1} – 20035cm^{-1}. 1983.

[13] S. Gerstenkorn and J. Verges. Atlas du spectre d'absorption de la molecule d'iode 7220 cm^{-1} – 11200cm^{-1}. 1982.

[14] S. Gerstenkorn, J. Verges, and J. Chevillard. Atlas du spectre d'absorption de la molecule d'iode 11000 cm^{-1} – 14000cm^{-1}. 1982.

[15] J. D Griffiths. *Introduction to Quantum Mechanics.* Pearson Education, Inc., 2nd edition, 2005.

[16] G. R. Hanes and C. E. Dahlstrom. Iodine hyperfine structure observed in saturated absorption at 633 nm. *Applied Physics Letters*, 14(11):362–364, 1969.

[17] G. Herzberg. *Molecular Spectra and Molecular Structure I. Spectra of Diatomic Molecules.* D. Van Nostrand Company, Inc., 2nd edition, 1950.

[18] D. Kielpinski, C. Monroe, and D. J. Wineland. Architecture for a large-scale ion-trap quantum computer. *Nature*, 417:709, 2002.

[19] H. Knöckel, B. Bodermann, and E. Tiemann. High precision description of rovibronic structure of the I_2 B-X spectrum. *Eur. Phys. J. D.*, 29:199 – 209, 2004.

[20] D.R. Lide. *CRC Handbook for Chemistry and Physics.* CRC Press, Inc., 88th edition, 2007.

[21] H. Ludvigsen and C. Holmlund. *Rev. Sci. Instrum*, 63:2135, 1992.

[22] D. N. Matsukevich, P. Maunz, D. L. Moehring, S. Olmschenk, and C. Monroe. Bell inequality violation with two remote atomic qubits. *Phys. Rev. Lett.*, to be published in 2008.

[23] H. J. Metcalf and P. Van der Straten. *Laser Cooling and Trapping.* Springer-Verlag, 1st edition, 1999.

[24] M.R. Matthews C.E. Wieman M.H. Anderson, J.R. Ensher and E.A. Cornell. Observation of bose-einstein condensation in a dilute atomic vapor. *Science*, 269(5221):198–201, 1995.

[25] D. L. Moehring, P. Maunz, S. Olmschenk, K. C. Younge, D. N. Matsukevich, L.-M. Duan, and C. Monroe. Entanglement of single-atom quantum bits at a distance. *Nature*, 449.

[26] A. Morinaga, K. Sugiyama, N. Ito, and J. Helmcke. Hyperfine structure of low-lying vibrational levels in the b electronic state of molecular iodine. *J. Opt. Soc. Am B*, 6(9), September 1989.

[27] S. Olmschenk, K. C. Younge, Matsukevich D. Moehring, D. L., P. Maunz, and C. Monroe. Manipulation and detection of a trapped yb+ hyperfine qubit. *Phys. Rev. A*, 76:052314, 2007.

[28] D. Porras and J. I. Cirac. Effective quantum spin systems with trapped ions. *Phys. Rev. Lett.*, 92(20):207901, May 2004.

[29] J. J. Sakurai. *Modern Quantum Mechanics.* Addison-Wesley Publishing Company, revised edition, 1994.

[30] B. E. A. Saleh and M. C. Teich. *Fundamentals of Photonics.* Wiley-Interscience, 2nd edition, 2007.

[31] A. E. Siegman. *Lasers.* University Science Books, 1st edition, 1986.

[32] Andrew M. Steane. How to build a 300 bit, 1 giga-operation quantum computer. 2004.

[33] D. J. Wineland, C. Monroe, W. M. Itano, D. Leibfried, B. E. King, and D. M. Meekhof. Experimental Issues in Coherent Quantum-State Manipulation of Trapped Atomic Ions. *J. Res. Natl. Inst. Stand. Technol.*, 103(3), 1995.